LIMNOLOGY and OCEANOGRAPHY: METHODS

ASLO

Limnol. Oceanogr.: Methods 13, 2015, 529–552

doi: 10.1002/lom3.10046

Estimating primary production from oxygen time series: A novel approach in the frequency domain

Tom J. S. Cox,*[1,2] Tom Maris,[2] Karline Soetaert,[1] Jacco C. Kromkamp,[1] Patrick Meire,[2] Filip Meysman[1]

[1]Department of Ecosystem Studies, Netherlands Institute of Sea Research (NIOZ-Yerseke) Korringaweg 7, 4400 AC Yerseke, The Netherlands

[2]Department of Biology, Ecosystem Management Research Group, University of Antwerp, Universiteitsplein 1, B-2610 Anwerpen, Belgium

Abstract

Based on an analysis in the frequency domain of the governing equation of oxygen dynamics in aquatic systems, we derive a new method for estimating gross primary production (GPP) from oxygen time series. The central result of this article is a relation between time averaged GPP and the amplitude of the diel harmonic in an oxygen time series. We call this relation the Fourier method for estimating GPP. To assess the performance and accuracy of the method, we generate synthetic oxygen time series with a series of gradually more complex models, and compare the result with simulated GPP. We demonstrate that the method is applicable in systems with a range of rates of mixing, air–water exchange and primary production. We also apply the new method to oxygen time series from the Scheldt estuary (Belgium) and compare it with ^{14}C-based GPP measurements. We demonstrate the Fourier method is particularly suited for estimating GPP in estuarine and coastal systems where tidal advection has a large imprint in observed oxygen concentrations. As such it enlarges the number of systems where GPP can be estimated from in situ oxygen concentrations. By shifting the focus to the frequency domain, we also gain some useful insights on the effect of observational error and of stochastic drivers of oxygen dynamics on metabolic estimates derived from oxygen time series.

Accurate rate estimates of whole ecosystem metabolism are crucial for our understanding of food web dynamics and biogeochemical cycling in aquatic ecosystems. Starting with the seminal work of Odum (1956), time series of in situ oxygen concentrations have been used to infer rates of gross primary production (GPP) and community respiration (CR) in natural waters (Staehr et al. 2010, 2012). This so-called diel oxygen method (also often referred to as the Odum method) tracks the oxygen concentration at a specific water depth over a 24 h cycle, and calculates GPP from the rate of change of oxygen during daylight hours, while adding the rate of community respiration determined at night (Howarth and Michaels 2000). The diel oxygen method has two main advantages over methods that rely on the ex situ incubation of water samples, such as the light-dark oxygen method (Riley 1939), ^{14}C-incorporation (Steemann Nielsen 1951) and ^{18}O-labeling (Grande et al. 1989). First, "bottle effects" are avoided: GPP and CR rates are obtained at ambient light fields, and natural levels of turbulence, nutrients and grazing; such conditions are hard to mimic in bottle incubation experiments. Second, upscaling bottle incubation GPP rates to depth integrated production depends on a range of assumptions about the in situ light field, and mixing of the water body (Swaney et al. 1999; Chen et al. 2000; Howarth and Michaels 2000; Staehr et al. 2010; Westberry et al. 2012).

There is, however, one major challenge associated with the in situ diel oxygen method: oxygen concentrations are not only affected by primary production and respiration but also by turbulent mixing, advective transport, and air–water exchange. Consequently, the effect of these transport processes on the rate of change of oxygen needs to be properly constrained, before one can confidently estimate GPP and CR. Mathematically, the diel oxygen method represents an inverse modeling problem, whereby GPP and CR are forcing functions in a differential equation that describes the oxygen mass balance of the aquatic system. These forcing functions can be constants or can be parameterized functions of observed incident irradiance and/or water temperature.

GPP and CR are determined by fitting this model to the available oxygen time series. When additional transport processes are included, the number of model parameters

*Correspondence: tom.cox@uantwerpen.be

increases, with each additional parameter introducing a new source of uncertainty. Therefore, the diel oxygen method works best in simple hydrodynamic settings where the influence of transport processes on the oxygen dynamics is small. The typical example is a closed pond system, where GPP and CR attain high values and are roughly equal, so oxygen gradients near the air–water interface are reduced and the resulting atmospheric exchange of oxygen is small (Marino and Howarth 1993). Yet in open systems with substantial gas exchange, estimates of ecosystem metabolism critically depend on the rate of reaeration, and the resulting GPP and CR values are highly sensitive to reaeration parameterizations (Tobias et al. 2009). Similarly, the diel oxygen method runs into trouble when advection and dispersion processes strongly influence the oxygen concentration, as small errors in the parameterization of these transport processes can lead to order-of-magnitude errors in resulting metabolic rates (Kemp and Boynton 1980).

In recent years, a number of extensions and refinements of the diel oxygen method have been adopted, so that the method performs better in aquatic systems with a strong imprint of transport processes. A first issue concerns the atmospheric exchange of oxygen, which can show strong temporal fluctuations, as a result of varying wind stress and associated changes in surface layer turbulence. Many recent studies calculate gas exchange rates from observed wind speed (Cole et al. 2000; Gelda and Effler 2002; Lauster et al. 2006; Tsai et al. 2008; Staehr et al. 2010; Coloso et al. 2011; Van de Bogert et al. 2012; Solomon et al. 2013). However, empirical reaeration parameterizations (e.g., the piston velocity as a function of wind speed) are dependent on the water body and local hydrodynamics, and so, it is difficult to determine a priori the piston velocity for a given water body (Tobias et al. 2009; Holtgrieve et al. 2010). To better constrain atmospheric oxygen exchange, one can include the reaeration rate as part of the inverse modeling problem, rather than fixing its parameter value a priori. This approach was employed by Ciavatta et al. (2008) to estimate GPP in the lagoon of Venice from a 3-yr time series of O_2 concentrations measured at 30 min intervals. Respiration and reaeration rates were estimated from O_2 data collected during night-time, while GPP data was subsequently estimated from O_2 data during the following day-time. To even better constrain atmospheric gas exchange, Holtgrieve et al. (2010) advocate the incorporation of a dual mass balance approach for the isotopes of dissolved oxygen ($\delta 18O-O_2$). Using a Bayesian inverse modeling approach, this method was successfully applied to a short ($\sim$24h) data series of South Saskatchewan River (Saskatoon, Canada). A second problem concerns the application of in situ diel techniques to systems in which advective transport has a strong impact on the oxygen dynamics. This is particularly relevant in rivers with complex flow patterns, or estuaries and coastal zones, where the water flow changes direction over a tidal cycle. One solution is to implement the in situ diel technique at multiple stations, and simply average the station results (Howarth et al. 1992). A more refined multistation approach was used by Swaney et al. (1999) to estimate GPP in the Hudson river, whereby O_2 concentrations were linearly regressed across stations as a function of depth, salinity and time. A more elaborate approach consists of the construction multidimensional oxygen mass balances. Vallino et al. (2005) used a 1D advection-dispersion model of the Parker River (Massachusets) to estimate GPP based on oxygen concentrations measured during high speed transects near dawn and dusk over a 2-d period.

Finally, arrays of oxygen sensors are increasingly deployed in systems with vertical or horizontal gradients [e.g., Gelda and Effler (2002); Coloso et al. (2008); Sadro et al. (2011); Champenois and Borges (2012); Van de Bogert et al. (2012); Obrador et al. (2014)]. For example, in clear, eutrophic, stratified lakes considerable photosynthesis can take place in the hypolimnion and the metalimnion. In one case study, Obrador et al. (2014) found that up to 20% of GPP can take place in the metalimnion. In such conditions any diel oxygen method will underestimate total GPP when applied to epilimnion O_2 time series only. The effect of stratification interacts with the trophic state of the system. Indeed, in oligotrophic systems, photosynthesis will be nutrient limited over a (large) part of the water column. When nutrient input and regeneration can be assumed independent of depth, also GPP would be independent of depth. Indeed, based on O_2 depth profiles taken in an oligotrophic lake at 2 h sampling interval, Sadro et al. (2011) concluded that single depth measurements are sufficient for metabolism estimates in such conditions. Horizontal homogeniety is even more important when diel oxygen methods are based on single sensor deployments. Van de Bogert et al. (2012) convincingly demonstrated that the assumption of horizontal homogeniety is often not met in lake ecosystems. Based on two case studies they found that single sensor derived GPP estimates varied over more than an order of magnitude between different locations.

Here, we examine a novel strategy to apply the diel oxygen method to aquatic systems that have a strong imprint of transport processes. The central idea is that different processes operate on different time scales, and so, they each will induce characteristic temporal fluctuations in the O_2 concentration. We start from the assumption that primary production is the dominant process that induces a 24 h periodicity in the oxygen signal—other processes will have their imprint at other frequencies. This calls for signal analysis in the frequency domain, whereby the oxygen signal is decomposed into a sum of individual frequency components. Kester et al. (1996) already demonstrated that the spectral analysis of oxygen time series data can provide relevant information on the different processes that affect the oxygen dynamics in natural waters. More recently, Coloso et al. (2008) and

Langman et al. (2010) applied wavelet techniques to separate the O_2-dynamics at different time scales. Here, we elaborate this idea by combining the diel oxygen method with spectral analysis. This results in a new Fourier-based method to estimate GPP from a time series of in situ oxygen sensor data. The principal difference with previous Odum-type methods is that our model analysis takes place in the frequency domain rather than the time domain. To test the accuracy and reliability of the method, we first verify the method with synthetic oxygen data generated by two separate biogeochemical models. Subsequently, we apply the method to a measured oxygen time series from an estuary and compare the resulting GPP values with primary production estimates based on ^{14}C-incorporation.

Material and methods

Theoretical background

Consider the typical situation where a single oxygen sensor is positioned in a given water body at water depth d_s. This sensor generates a time series of the oxygen concentrations over a time period T at regular intervals Δt (Fig. 1). The mass balance for oxygen over a suitable control volume surrounding the sensor can be written as:

$$\frac{d\mathrm{O}_2(t)}{dt} = \mathrm{GPP}(t) - \mathrm{CR}(t) + \frac{1}{V}\int_{\partial V} \mathrm{F}(t) \cdot d\mathrm{S} \qquad (1)$$

In this, O_2 denotes the average oxygen concentration in the control volume, GPP and CR are respectively the volume-averaged gross primary production and community respiration, V represents the volume. The last term is a surface integral that integrates the flux F due to advection and diffusion across the boundary of the control volume. Note that this mass balance statement does not adopt any simplifying assumptions: it is generally valid, even for systems that are not homogeneously mixed.

The above differential equation specifies the oxygen mass balance in the time domain. An entirely equivalent description is possible in the frequency domain by taking the Fourier transform

$$i\omega\mathcal{F}(\mathrm{O}_2)(\omega) = \mathcal{F}(\mathrm{GPP})(\omega) - \mathcal{F}(\mathrm{CR})(\omega) + \frac{1}{V}\int_{\partial V} \mathcal{F}(\mathrm{F})(\omega) \cdot d\mathrm{S} \qquad (2)$$

In this, $\mathcal{F}(f)(\omega)$ denotes the Fourier transform of the function *f(t)*, ω is the angular frequency, and i represents the imaginary unit [*see* Folland (1992) and Bloomfield (2000) for details on Fourier transforms]. When $f(t)$ is a time varying signal, the Fourier transform decomposes this signal into different periodic components, whereby $|\mathcal{F}(f)(\omega)|$ is the *amplitude* of the periodic component with angular frequency ω. In essence, the transformed mass balance specifies how strongly the various processes (on the right-hand side) contribute to the rate of change of oxygen (the term on the left-hand side) at any given frequency.

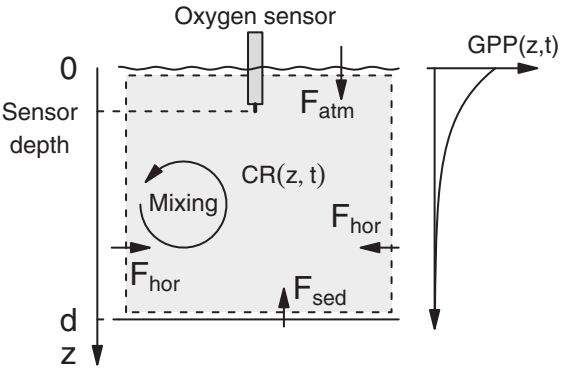

Fig. 1. A typical setup. The average oxygen concentration in a certain control volume (grey area) is determined by the balance of production (GPP), consumption (CR) and the fluxes through the boundaries of the volume. The distribution of the oxygen concentration within the control volume is also determined by mixing dynamics.A sensor measures the oxygen concentration at certain depth.

The central idea in our analysis is that gross primary production is the dominant process that causes diurnal variations in the oxygen concentration. Therefore, we specifically evaluate Eq. 2 at the diurnal frequency $\omega_1 = 2\pi$ rad d^{-1}. In addition, we can further simplify Eq. 2 based on three assumptions.

1. We assume that respiration does not induce substantial oxygen fluctuations at the diurnal frequency ω_1. Note that in reality respiration somtimes does exhibit diurnal patterns: higher water temperatures during daytime will induce diurnal fluctuations in bacterial activity; light sensitivity of nitrifying bacteria can induce diurnal fluctuations in nitrification rates (Guerrero and Jones 1996); and respiration by autotrophs can be higher during daytime (Markager and Sand-Jensen 1989). From oxygen data alone, the effect of higher oxygen consumption rates during day-time cannot be distinguished from lower gross primary production rates, and neglecting this effect will, hence, result in an underestimation of gross primary production. However, this underestimation is generally assumed to be small and in nearly all applications of the diel oxygen method diurnal fluctuations in community respiration are neglected (Staehr et al. 2010).
2. We assume that fluxes through the boundary of the control volume do not show any systematic diurnal fluctuations. This is not a trivial assumption. Diurnal fluctuations in oxygen concentration induced by primary production will also induce diurnal fluctuations in atmospheric exchange. Also, when horizontal oxygen gradients are present in estuarine and coastal systems, the diurnal component of the tides will induce diurnal fluctuations in the horizontal oxygen fluxes. Horizontal gradients in

primary production will have similar effects. The importance of diurnal fluctuations in boundary fluxes, and ther impact on the GPP estimate, will be evaluated by means of a theroretical analysis (for air–water exchange) and by the model simulations below.

3. The water body is homogenously mixed and concentration gradients are annihilated. This way, oxygen concentrations measured by a single sensor will be represenative for the volume averaged oxygen concentrations. This assumption of homogeneity underlies most in situ diel oxygen methods (Staehr et al. 2010). When it is not met, time series of volume averaged oxygen concentrations can be estimated with an array of sensors.

Based on the above assumptions [1] and [2], we can simplify Eq. 9 as:

$$i\omega_1 \mathcal{F}(O_2)(\omega_1) = \mathcal{F}(GPP)(\omega_1) \quad (3)$$

Taking the modulus and introducing the shorthand notation $A_f = |\mathcal{F}(f)(\omega_1)|$ for the amplitude at the diurnal frequency:

$$\omega_1 A_{O_2} \approx A_{GPP} \quad (4)$$

The quantity A_{O_2} represents the Fourier amplitude at the diurnal frequency of the volume-averaged oxygen signal, which can be directly determined from oxygen sensor recordings (assuming that the sensor truly records the volume-averaged oxygen signal). The quantity A_{GPP} is the Fourier amplitude of gross primary production at the diurnal frequency. This quantity in itself is not a meaningful ecological parameter. To be useful, A_{GPP} needs to be linked to the time-averaged value of GPP over some time period T. To this end, we need an explicit model of how GPP varies over a daily cycle. For simplicity, we assume here that the daily fluctuating GPP follows a truncated sinus function, with a smoothly varying production during daylight and no production at night (Fig. 10). For a truncated sinusoid, an exact relation exists between its time-averaged value and its Fourier-transformed amplitude at diurnal frequency (*see* Appendix). If we apply this relation to GPP, and combine this with Eq. 9, we arrive at the following approximation of time averaged gross production

$$\overline{GPP(t)} \approx 2\omega_1 \frac{\sin\theta - \theta\cos\theta}{\theta - \frac{1}{2}\sin 2\theta} A_{O_2} \quad (5)$$

The parameter $\theta = \pi f_{DL}$, with f_{DL} the relative fraction of daylight hours over a 24 h period (Fig. 10). This parameter can be determined from observed incident light or alternatively from the theoretical day length at a given Julian day and a given position on the globe (Anonymous 2011). The quantity ω_1 denotes the diurnal frequency as introduced above. When the fraction of daylight hours f_{DL} decreases, the factor in front of A_{O_2} decreases, and so the time-averaged GPP also decreases. The factor in front of A_{O_2} varies between 0.5 and 0.8 if f_{DL} ranges between 30% and 70%. Note that if we would approximate GPP by a nontruncated sinusoid, $f_{DL} = 1$ and this factor equals unity.

Equation 5 forms the central result of this article. It will be applied in the next sections to both synthetic and field data. We will refer to the associated procedure as the *Fourier method* for estimating GPP.

Impact of air–water exchange

Can we neglect diurnal fluctuations in air–water exchange? To this end, we consider a horizontally homogeneous water column, where lateral fluxes and bottom fluxes (at the sediment interface) show no diurnal fluctuations. The classical rate expression for atmospheric exchange flux is given by:

$$F_{atm} = k(O_2^{sat} - O_2(z=0)) \quad (6)$$

where k is the piston velocity and O_2^{sat} the saturation concentration of a water body in equilibrium with the atmosphere, and $O_2(z=0)$ the oxygen concentration at the air–water interface. If we include this air–water flux, Eq. 2 evaluated at the diurnal frequency then reduces to

$$i\omega_1 \mathcal{F}(O_2)(\omega_1) + \frac{k}{d}\mathcal{F}(O_2(z=0))(\omega_1) = \mathcal{F}(GPP)(\omega_1) \quad (7)$$

where we also assumed that diurnal variability in the piston velocity due to wind speed variability and temperature induced diurnal fluctuation in oxygen saturation are negligible. The left-hand side of this equation depends on the oxygen concentration at the air–water interface, and this is dependent on the mixing dynamics of the water body. When mixing is fast and the water column can be considered perfectly mixed, the concentration at this interface will equal the depth averaged oxygen concentration, and so:

$$\left(i\omega_1 + \frac{k}{d}\right)\mathcal{F}(O_2)(\omega_1) = \mathcal{F}(GPP)(\omega_1) \quad (8)$$

Taking the modulus, we, hence, obtain:

$$\omega_1 \sqrt{1 + \left(\frac{k}{\omega_1 d}\right)^2} A_{O_2} = A_{GPP} \quad (9)$$

The term $\frac{k}{\omega_1 d}$ reflects the dampening of the oxygen variations in the water column, due to atmospheric exchange. Equation 9 gives a first order correction to account for this dampening. This correction is often small. Indeed, consider a shallow 5 m deep lake with relatively low turbulence (low piston velocity $k = 0.5$ m d^{-1}), we have $\frac{k}{\omega_1 d} \approx 0.016$, and the resulting correction in Eq. 9 is smaller than 0.02%. For an estuarine or coastal system of 10 m depth, with a high piston velocity ($k = 3.5$ m d^{-1}), the correction factor amounts to

0.3%, which is still small. Note that these results are based on the assumption of a fully mixed water column, and should be considered as minimal estimates. In reality water columns are not perfectly mixed and atmospheric exchange will affect the upper water layers more than the deeper layers. The upper layer is also where primary production production takes place, and hence, oxygen concentration fluctuations are greatest. Therefore, in systems that are not perfectly mixed, the dampening-effect of atmospheric exchange will be larger than calculated above. The effect is will be assessed in more detail in the model simulations below.

When the dampening effect due to air–water exchange is included, formula 5 for GPP extends to:

$$\overline{\mathrm{GPP}(t)} \approx 2\omega_1 \frac{\sin\theta - \theta\cos\theta}{\theta - \frac{1}{2}\sin 2\theta} \sqrt{1 + \left(\frac{k}{2\pi d}\right)^2} A_{\mathrm{O}_2} \tag{10}$$

Signal processing

To calculate the Fourier amplitude A_{O_2} from such a time series, we implemented some data preprocessing steps. These processing steps are not specific to the present application but are generally applied when numerically calculating Fourier transforms from finite length time series (Bloomfield 2000). First, the oxygen time series is confined to an integer number of days. Second, longer trends are removed with a moving average filter. A moving average filter is, however, not perfect: while removing the longer-term trends, it will also affect the shorter term fluctuations to some extent. To compensate for this, a correction factor can be applied, based on the frequency response of the moving average filter (Folland 1992; Bloomfield 2000).

$$H(\omega, N) = \frac{1}{N} \frac{1 - \exp(-i\omega N)}{1 - \exp(-i\omega)} \tag{11}$$

where N is the filter length. At the diurnal frequency ω_1, the Fourier amplitude $A_{\mathrm{O}_2} = \mathcal{F}(\mathrm{O}_2)(\omega_1)$ will be attenuated by the factor $|1 - H(\omega_1, N)|$ as a result of the moving average filter. To correct for this, we multiplied the Fourier amplitude obtained from filtered time series with the inverse of this attenuation factor.

The common approach to isolate a periodic component with known frequency from a composite signal is to perform a least-squares fit a sinusoid with that frequency and unknown phase and amplitude to the time series (Bloomfield 2000). For Fourier frequencies, the solution of the least-squares fit is identical to the corresponding component of the Fourier transform of the time series (Bloomfield 2000). By limiting the time series to an integer number of days, the diurnal frequency becomes a Fourier frequency and, thus, we calculate A_{O_2} directly from the definition of the Fourier transform as

$$A_{\mathrm{O}_2} = \left| \sum_{n=1}^{L} \exp(-i\omega_1 t_n) \mathrm{O}_2(t_n) \right| \tag{12}$$

where L is the length of the time series, and t_n are the sampling times. The Fourier method, thus, does not make use of the fast fourier transform (FFT). Only for plotting the spectra in this manuscript, FFT was applied to the preprocessed time series. All data processing was performed in R (R Development Core Team 2006).

Model simulations to assess the simplifying assumptions

In comparison to the classical diel oxygen method, two additional assumptions are crucial in the derivation of the Fourier method. First, the truncated sinusoid approximation requires that the relation between time averaged GPP and the Fourier amplitude is approximately the same as for a truncated sinusoid. Second, diurnal fluctuations in fluxes through the boundaries of the water body are assumed to be negligible. We assess these assumptions by analysing a set of three, gradually more complex models of GPP and oxygen dynamics. We first study the behavior of an idealized pond model with real incident light in a perfectly mixed water column with constant algal biomass, where we assume GPP can be observed directly. This allows for a first assessment of the truncated sinusoid approximation. Next we analyse two dynamic models: the first one describes a water body with no appreciable lateral transport of oxygen, representative for a lake or the surface layer of the ocean, where vertical turbulence and air–water exchange are the dominant transport processes. The second describes a typical estuarine situation, characterized by substantial horizontal gradients in the O_2 concentration. The next sections describe these models in detail; full model equations are given in Table 1. The dynamic models generate time series of oxygen concentrations. The temporal resolution was kept similar as in typical field recordings of oxygen (Δt=10 min resolution). These synthetic oxygen data were then supplied to the Fourier method and treated in a identical way as field sensor data. The resulting Fourier-based estimate of the GPP was then compared to the true GPP as obtained from the model simulation. This procedure allowed to systematically test the underlying assumptions of the Fourier method.

Idealized pond model

In general, depth integrated GPP is a nonlinear function of the light field in the water column. This light field follows an irregular pattern over time, and so will GPP. Within a single day the light field fluctuates as a results of changing weather conditions and turbidity variations that affect the light availability in the water column. These will lead to fluctuations in photosynthetic activity. Changing weather conditions also induce variability between consecutive days of the incident irradiance. In the idealized pond model we assume a Platt-type response of photosynthesis to irradiance characterized by a maximal photosynthetic rate P_m and a

light saturation parameter $E_m = P_m/\alpha$ (Jassby and Platt 1976). Furthermore we assume light extinction with water depth z is described by the exponential Lambert-Beer law using a fixed light attenuation coefficient k_d. The model is forced with observed time varying surface irradiance $E_0(t)$ (*see* below). Finally, the algal biomass B is kept constant. This strong simplification is relaxed in the subsequent dynamic models.

With this model, we calculated 14-d long time series of depth-averaged GPP (assumed to be directly observable) from observed incident irradiance. We did so for each subset of 14 consecutive days (351 subsets) in a full year of hourly irradiance data recorded in 2009 on the roof of NIOZ-Yerseke (Nl.) using a Licor LI-190 SA cosine sensor. We determined the Fourier amplitude at the diel frequency of each of these GPP time series, from which the estimate of time averaged GPP was calculated using formula 23 in the Appendix. Comparing these estimates with true time averaged GPP effectively tests to what extent the truncated sinusoid assumption holds.

The difference between true time averaged GPP and the estimate from the Fourier-amplitude at the diel frequency depends on the nonlinearity of the response. In the idealized pond model,this nonlinearity is determined by the parameters E_m and k_d. We repeated the above procedure for $E_m = 50$, 100, 250, 500 μmol photons $m^{-2}s^{-1}$ and for $k_d = 0.1$, 1, 2 and $100\,m^{-1}$. Note that, when assuming a Lambert–Beer exponential light attenuation in the water column, the depth integrated GPP scales with the light attenuation coefficient k_d as long as the mixing depth of the system is higher than the light penetration depth. In that case, the upper limit of the integral can be set to ∞, and we can substitute the dummy integration variable z by $\tilde{z} = k_d z$. Consequently, at large values of k_d relative to the system depth, the relative bias is independent of k_d. GPP also scales with B, assumed here constant in time. Thus, also the value of B does not affect the relative bias.

Open water model

The open water model dynamically simulates oxygen and algal biomass in a vertical water column. This relaxes the assumption of constant biomass. A finite vertical mixing rate allows for concentrations gradients in the vertical. Air–water exchange is implemented to generate a flux accross the upper boundary of the model domain. We still assume that oxygen fluxes at the lower boundary (e.g., due to sediment oxygen uptake) and lateral boundaries can be ignored.

The model is implemented as a one-dimensional reactive transport model that incorporates two state variables, O_2 and B. The water column has a total depth $d = 10\,m$, and the coordinate z represents the distance from the air–water interface. The model is integrated on an equidistant grid with distance between grid points $\Delta z = 0.25\,m$.

Oxygen is produced by primary production (GPP), and consumed by respiration (CR). Oxygen and algal biomass are transported throughout the vertical by turbulent mixing (vertical diffusion constant D). Primary production is modelled via a Platt-type photosynthesis-irradiance relationship. The light attenuation with depth is described by the exponential Lambert–Beer law, using a fixed attenuation coefficient k_d.

The exchange of oxygen with the atmosphere is implemented via the standard rate expression, that is, the degree of O_2 undersaturation times the piston velocity k. At the bottom of the water column, the oxygen flux vanishes (benthic consumption is neglected). Similarly, the algal fluxes are zero at the upper and lower boundary.

The model was forced with observed surface irradiance $E_0(t)$ as in the idealized pond model. The model simulation output consisted of depth profiles of oxygen, algal biomass and volumetric GPP through time. From the model output depth averaged oxygen time series were calculated. Similarly, recordings of a virtual oxygen sensor situated at depth d_s were obtained by extracting the corresponding O_2 output from the simulation output. From these oxygen time series, we calculated the GPP by the Fourier method (average GPP over moving 14 d intervals). At the same time, we calculated the true GPP values by suitably averaging the simulated GPP rate over the depth of the model domain and the associated 14 d period.

We assessed the effect of neglecting diurnal fluctuations in air–water exchange when the water column is not perfectly mixed. From the model output, we calculated the relative underestimation $\omega_1 A_{O2}/A_{GPP} - 1$. We calculated this underestimation with incident irradiance observed in the first two weeks of June. These weeks have most sunshine, and consequently primary production is highest. During this period vertical oxygen gradients will be highest, and, thus, also the effect of imperfect mixing on air–water exchange. For the same reason, we fixed the light attenuation coefficient to a large value of $10\,m^{-1}$.

Diurnal fluctuations in air–water exchange are influenced by the rate of exchange (piston velocity) and mixing (turbulent diffusion coefficient). Therefore, we ran the model over a suitable range of piston velocities (0.5, 3.5, and $5\,m\,d^{-1}$) and turbulent diffusion coefficients (10^{-2}, 5.10^{-3}, and 10^{-3} $m^2\,s^{-1}$). These span a range from lakes with low wind speeds and reduced turbulence to estuaries and coasts where higher wind speeds and water currents significantly increase the piston velocity and turbulence (Borges et al. 2004a, 2004b; Staehr et al. 2010).

Estuary model

The estuary model is of comparable biogeochemical complexity as the open water model, but relaxes different assumptions. As a result of the tidal energy dynamics, it is assumed that vertical mixing is intense, so that all solutes

Table 1. Balance equations, process rates, boundary conditions and forcing functions for the models with which synthetic oxygen time series were generated. The open water and estuary model inherit the rate formulation of GPP and forcing function from the idealized pond model

Idealized pond model		
Process rate		
Gross primary production		
$\mathrm{GPP}(t)$	=	$\frac{B}{d}\mu(t)$
$\mu(t)$	=	$\int_0^d \mu(z,t)dz$
$\mu(z,t)$	=	$\mathrm{P_m}\left(1-\exp\left(-\frac{\alpha E(z,t)}{P_m}\right)\right)$
$E(z,t)$	=	$E_0(t)\exp(-k_d z)$
Forcing functions		
$E_0(t)$	:	Incident irradiance (hourly observations)
Open water model		
Balance equations		
$\frac{\partial}{\partial t}\mathrm{O_2}(z,t)$	=	$\mathrm{GPP}(z,t)-\mathrm{CR}(z,t)+\frac{\partial}{\partial z}\left(\mathrm{D}\frac{\partial}{\partial z}\mathrm{O_2}(z,t)\right)$
$\frac{\partial}{\partial t}\mathrm{B}(z,t)$	=	$\mathrm{C}:\mathrm{O_2}(\mathrm{GPP}(z,t)-\mathrm{CR}(z,t))+\frac{\partial}{\partial z}\left(\mathrm{D}\frac{\partial}{\partial z}\mathrm{B}(z,t)\right)$
Process rates		
Gross primary production		
$\mathrm{GPP}(z,\ t)$	=	$\mu(z,\ t)B(z,\ t)$
Community respiration		
$\mathrm{CR}(z,\ t)$	=	$R_m\mathrm{B}(z,\ t)$
Boundary conditions		
$-\mathrm{D}\frac{\partial}{\partial z}\mathrm{O_2}(z,t)\vert_{z=0}$	=	$k\left(\mathrm{O_2^{sat}}-\mathrm{O_2}(0,t)\right)$
$-\mathrm{D}\frac{\partial}{\partial z}\mathrm{O_2}(z,t)\vert_{z=d}$	=	0
$-\mathrm{D}\frac{\partial}{\partial z}\mathrm{B}(z,t)\vert_{z=0,z=d}$	=	0
Estuary model		
Balance equations		
$\frac{\partial}{\partial t}\mathrm{O}_{2(x,t)}$	=	$\mathrm{GPP}(x,t)-\mathrm{CR}(x,t)-r_{ODU}\mathrm{ODU}(x,t)+F^{\mathrm{A}}(t)/d+\frac{\partial}{\partial x}\left(\mathrm{D_x}\frac{\partial}{\partial x}\mathrm{O_2}(x,t)\right)-v\frac{\partial}{\partial x}\mathrm{O_2}(x,t)$
$\frac{\partial}{\partial t}\mathrm{B}_{(x,t)}$	=	$\mathrm{C}:\mathrm{O_2}\left(\mathrm{GPP}(x,t)-\mathrm{CR}(x,t)+\frac{\partial}{\partial x}\left(\mathrm{D_x}\frac{\partial}{\partial x}\mathrm{B}(x,t)\right)\right)-v\frac{\partial}{\partial x}\mathrm{B}(x,t)$
$\frac{\partial}{\partial t}\mathrm{ODU}(x,t)$	=	$-r_{ODU}\mathrm{ODU}+\frac{\partial}{\partial x}\left(\mathrm{D_x}\frac{\partial}{\partial x}\mathrm{ODU}(x,t)\right)-v\frac{\partial}{\partial x}\mathrm{ODU}(x,t)$
Process rates		
Gross primary production		
$\mathrm{GPP}(x,\ t)$	=	$\mu\ (t)\mathrm{B}(x,\ t)$
Community respiration		
$\mathrm{CR}(x,\ t)$	=	$R_m\mathrm{B}(x,\ t)$
Boundary conditions		
$\mathrm{ODU}(0,\ t)$	=	ODU^{up}
$\frac{\partial}{\partial x}\mathrm{ODU}(x,t)\vert_{x=L}$	=	0
$\mathrm{O_2}(0,t)$	=	$\mathrm{O_2^{up}}$
$\frac{\partial}{\partial x}\mathrm{O_2}(x,t)\vert_{x=L}$	=	0
$\mathrm{B}(0,\ t)$	=	B^{up}
$\frac{\partial}{\partial x}\mathrm{B}(x,t)\vert_{x=L}$	=	0

are mixed homeneously over the water column at all times. However, the lateral exchange of oxygen is considered important, giving rise to concentration gradients in the horizontal. Air–water exchange is explicitly incorporated, while oxygen fluxes across the lower boundary are ignored (no sedimentary oxygen consumption). In such an estuarine setting, oxygen recordings at a fixed location have an important imprint of the tidal oscilation of water masses passing by the sensor.

The estuary model is implemented as a one-dimensional reactive transport model, which simulates a stretch of length L, subject to tidal advection (streamwise velocity v), and dispersion (streamwise turbulent diffusifvity D_x). Lateral exchange is assumed negligible. In addition to oxygen and

Table 2. Process parameters and boundary conditions that were fixed throughout this study. Variable parameters are discussed in the text

O_2^{sat}	=	250	mmol m^{-3}
R_m	=	0.25	d^{-1}
$C:O_2$	=	1	mmol C (mmol O_2)$^{-1}$
C:Chl	=	20	mg C (mg Chl)$^{-1}$
r_{ODU}	=	.05	d^{-1}
v		2160	m d^{-1}
D_x	=	8.64 10^6	m^2 d^{-1}
d	=	10	m
ODU^{up}	=	200	mmol O_2 m^{-3}
B^{up}	=	10	mg Chl m^{-3}
O_2^{up}	=	100	mmol O_2 m^{-3}

algal biomass, the model includes a reduced compound (the oxygen demand unit [ODU]) as an additional state variable. This formulation provides a generic way to account for any bacterial and chemical oxygen consumption in the water (Soetaert et al. (1996). The removal of oxygen through the oxidation of ODU is modeled as a first order process in the ODU concentration. Primary production, respiration, and the incident light forcing are implemented similarly as in the open water model. A 100 d spin-up period was used to obtain proper initial conditions for the state-vectors of O_2, B and ODU along the x-axis.

The model simulation output consisted of transect profiles of oxygen, algal biomass, ODU and areal GPP through time. Solute transport in the estuary is modeled in a reference frame moving with the tides. Consequently, a sensor located at a fixed geographical position will oscillate horizontally in this reference frame. Therefore, the output of the model is resampled with a virtual, horizontally oscillating sensor. The resampling procedure is described in detail in the Appendix.

The resulting oxygen data corresponds to what a sensor would record in a real estuarine setting where water masses are moving along the sensor with the tides. From this oxygen time series, we calculated the GPP by the Fourier method (average GPP over moving 14 d intervals). The GPP rates were resampled in an identical way, from which true time averaged GPP was calculated.

The estuarine model explicitly accounts for the effect of lateral transport on the GPP estimates. To *see* how important these are, we can estimate the error made by neglecting diel fluctuations in horizontal fluxes. These may arise from the diurnal component of the tides in the presence of horizontal oxygen gradient or from horizontal gradients in primary production. From the model output, we can specifically calculate the relative contribution of the advective term $-v\frac{\partial O_2}{\partial x}$ to this error. By calculating the Fourier transform of this term, it is possible to correct the Fourier-based GPP for diel fluctuations in advective flux. We did this for each simulation. To evaluate this simulation result, we compared it with a partial approximation of the Fourier amplitude of the advective term, based on in situ time series of salinity and concentration gradients of oxygen and salinity (the full details of the procedure are given in the Appendix).

Parameter values implemented in the model simulations are based on the site where the field data were collected (Schelde estuary—*see* below). The full model equations are found in Table 1, while the values of parameters that were fixed in all simulations can be found in Table 2. The models where numerically integrated with a standard solver from the R-package deSolve, making use of the upstream weighted differencing schemes for the transport equations as defined in the package ReacTran (Soetaert et al. 2010; Soetaert and Meysman 2011). R scripts are available on request.

Comparison to field data

Oxygen time series data were collected at a fixed geographical location (Kruibeke: 51°10′33″N, 4°19′32″O) in the upper brackish part of the Schelde estuary (Belgium). The average tidal amplitude at this site is 5.3 m, the mean depth of the water column is about 9.3 m. Tidal currents are strong: maximal water velocity during an average tidal cycle is 1.2–1.3 m s^{-1}. Tidal excursion at this location is estimated 10–20 km. The oxygen concentration features strong horizontal gradients in this part of the estuary due to intense mineralization and nitrification (Van Damme et al. 2005; Soetaert et al. 2006).

In 2010, O_2 concentrations were recorded from a pontoon with three equivalent sensor configurations (Fig. 9): a Hydrolab Datasonde multiprobe logger mounted with a Clark type sensor and a YSI 6600ADV multiparameter sonde mounted with either a Clark type sensor or an optical sensor (ROX, YSI). Oxygen was recorded at a constant depth of 0.75 m below the water surface, over periods of 10–30 d, with a sampling interval of 10 min.

^{14}C-incubation measurements of primary production were conducted on water samples taken shipboard in the central part of the river at the location of the pontoon. Samples were incubated for 2 h. Dark bottle incubations were used to correct for chemosynthetic processes. Maximum photosynthetic rate P_m and photosynthetic efficiency α were determined from Eilers–Peeters curves fitted to observed photosynthesis-irradiance data couples (Eilers and Peeters 1988). Depth-integrated primary production was calculated using hourly incident irradiance. Light attenuation is highly variable near the study site (Desmit et al. 2005). At slack tide, suspended sediments settle down quickly causing a short period low light attenuation, while high peaks in light attenuation are often observed. Therefore, we chose not to use observed light attenuation coefficient during sampling,

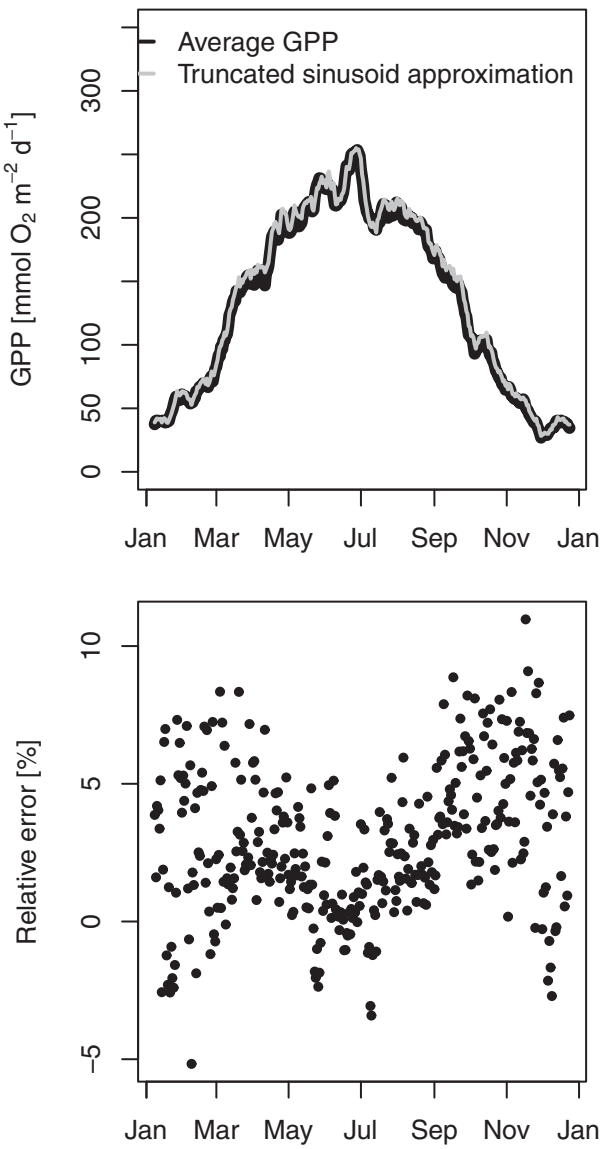

Fig. 2. Depth averaged GPP and truncated sinusoid approximation, calculated with the idealized pond model for all subsets of 14 consecutive days of observed irradiance (top panel). Relative error (bottom panel)

but we set k_d to a typical value of $4.5\,m^{-1}$. This avoids unrealistic high or low production estimates in cases that sampling was performed during peak periods of light attenuation.

Production between sampling days was interpolated using measured irradiance data and assuming that other parameters (Chlorophyll *a* [Chl *a*], photosynthetic parameters) did not change during the calculation interval. Hourly irradiance data was measured with the Licor LI-190 SA cosine sensor at the roof of the NIOZ institute (*see* above). For further details on sampling procedures, materials and methods *see* Kromkamp and Peene (1995).

Table 3. Relative difference between truncated sinusoid approximation and 14 d average of GPP calculated with the idealized pond model. Water depth 10 m. Average and standard deviation calculated for all consecutive 14 d intervals in 2009. Units E_m: μmol photons $m^{-2}s^{-1}$; k_d: m^{-1}

	k_d			
E_m	**0.1**	**1**	**2**	**100**
50	−13 ± 9%	−9 ± 8%	−3 ± 5%	−3 ± 5%
100	−8 ± 8%	−4 ± 6%	−0.6 ± 4%	−0.6 ± 4%
250	−2 ± 5%	1 ± 4%	3 ± 4%	3 ± 4%
500	2 ± 4%	4 ± 4%	5 ± 4%	5 ± 4%

Results

Idealized pond model

Figure 2 shows the relative difference between the truncated sinusoid approximation and the 14 d average of depth averaged GPP, calculated with idealized pond model. The figure was generated with parameter values $k = 2\,m^{-1}$, $E_m = 250$ μmol photons $m^{-2}s^{-1}$ and $d = 10\,m$. The relative bias between true GPP and Fourier based GPP is calculated as

$$\text{bias} = 100 \times (\text{GPP}_{\text{Fourier}} - \text{GPP}_{\text{true}})/\text{GPP}_{\text{true}} \qquad (13)$$

The truncated sinusoid approximation overestimates real GPP with 3 ± 3.4%, and there is a weak seasonality: in winter months both the upward bias and the variability are slightly larger.

Subsequently, we performed a sensitivity analysis, changing the light saturation parameter E_m and light attenuation factor O_2. The values for E_m span a range observed in open oceans (Sarthou et al. 2005), coastal zones (Shaw and Purdie 2001), estuaries (Harding et al. 1986; Kromkamp and Peene 1995) and, lakes (Fahnenstiel et al. 1989). The k_d-values range from clear water (k_d=0.1 m^{-1}) to extremely turbid (k_d=100 m^{-1}). Note that the light attenuation factor and the water depth do not feature as independent parameters in the GPP-equation (*See* Table 1). In the simulations, we, hence, fixed the water depth at 10 m and only varied k_d.

The results of this sensitivity analysis are shown in Table 3. In all but one combination of parameter values, the bias is less than 10%. When $k_d > 2\ m^{-1}$, which is the case in many coastal and estuarine systems, the bias is at most 5% in absolute value. The results in Table 3 are identical for $k_d = 2\,m^{-1}$ and $k_d = 100\,m^{-1}$. This illustrates the fact that the relative difference is unaffected by k_d as long as the mixing depth of the system is larger than the light penetration depth.

Open water model

From here on we will focus our attention to coastal and estuarine systems where classical diel oxygen methods are often inapplicable. With the vertical water column model, we repeated the above procedure to calculate the relative

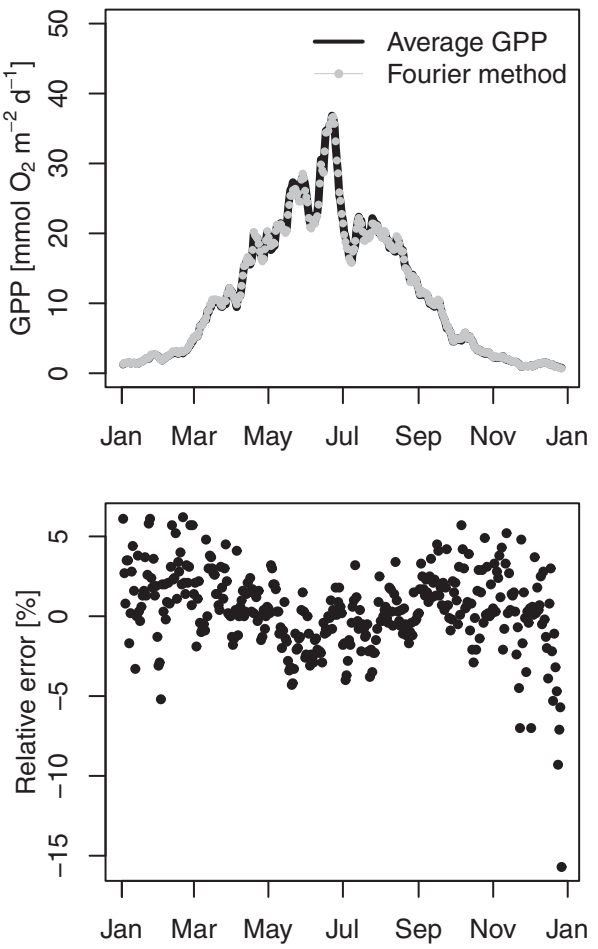

Fig. 3. Simulated GPP and Fourier method applied to O_2-series from the vertical water column model. The model was forced with all subsets of 14 consecutive days of observed irradiance (top). Relative mismatch between average GPP and Fourier estimate (bottom).

difference between the truncated sinusoid approximation and the 14 d average of depth averaged GPP. Figure 3 shows results from the simulations with depth = 10 m, vertical turbulent diffusivity = 10^{-2} m^2s^{-1} and light attenuation = 4.5 m^{-1}. With these parameter settings the Fourier method, applied to depth averaged simulated oxygen concentrations, accurately estimates the true GPP (bias of 0.4±2.5%.) Also here, a weak seasonality is observed: in winter months both the upward bias and the variability are slightly larger (Fig. 3).

From the model output, we also calculated the effect of the truncated sinusoid approximation, where now algal biomass is not constant but dynamically simulated. Interestingly, bias and random error amount to 2.6±2.8% and are lower than calculated from the idealized pond model with fixed biomass in the previous section. Or: dynamically simulated GPP in a vertical water column behaves more like a truncated sinusoid than depth integrated GPP with constant biomass. Note also that the bias in the Fourier method, on average 0.4%, is lower than the one introduced by the sinusoid approximation which is on average 2.6%. This can partly be ascribed to the effect of air–water exchange damping the oxygen signal; indeed, this damping decreases the amplitude of diel oscilations in oxygen and, therefore, decreases the bias in the Fourier method.

Table 4. Underestimation of GPP due to neglecting diurnal fluctuations in air–water exchange as estimated with the vertical water column model, for different values of vertical turbulent diffusion *D* and piston velocity *k*. Water depth was set to 10 m. The model was forced with incident irradiance observed in the first two weeks of June 2009. Units *D*: m^2 s^{-1}; *k*: m d^{-1}; k_d: m^{-1}

		k		
	D	**0.5**	**3.5**	**5**
$k_d = 10$	10^{-2}	−0.19%	−1.4%	−2.1%
	5.10^{-3}	−0.37%	−2.6%	−3.8%
	10^{-3}	−1.4%	−9.3%	−13%
	10^{-4}	−3.8%	−24%	−31%
$k_d = 1$	10^{-2}	−0.098%	−0.82%	−1.3%
	5.10^{-3}	−0.18%	−1.4%	−2.1%
	10^{-3}	−0.53%	−3.9%	−5.7%
	10^{-4}	−0.34%	−4.1%	−6.4%
	10^{-6}	−0.75%	−12%	−16%

The results of the model simulation for different piston velocities and vertical mixing rates are shown in Table 4. In the turbid water simulations (k=10 m^{-1}), the underestimation ranges from 0.19% in the fastest mixing system with lowest piston velocity to 31% in the slowest mixing system with highest piston velocity. Note that the combination of high piston velocity and low vertical mixing rate (or vice versa) is rather unphysical. The highest piston velocities are representative for systems with high wind speeds and water currents, where vertical mixing will also be high. Remind also that the light attenuation coefficient O_2 and the light forcing were chosen such to have maximal underestimation. Underestimation is much lower in the clear water simulations (k=1 m^{-3}). Underestimation now ranges from 0.098% to 16%, with the lowest vertical turbulent diffusivity in the clear water simulation a factor hundred lower than in the turbid water simulations. Even for the fastest mixing system, the simulated dampening is significantly larger than the theoretical correction factor (Eq. 9). For example, for a piston velocity of 3.5 m s^{-1} and a depth of 10 m this theoretical correction factor is only 0.16%: a factor 10 lower than the turbid water simulation result and a factor 5 lower in the clear water simulation both with $D = 10^{-2}\,m^2\,s^{-1}$.

The above analysis assumes that we have an ideal sensor, or a sensor array, which truly records the average oxygen concentration in the model domain (and, hence, the oxygen

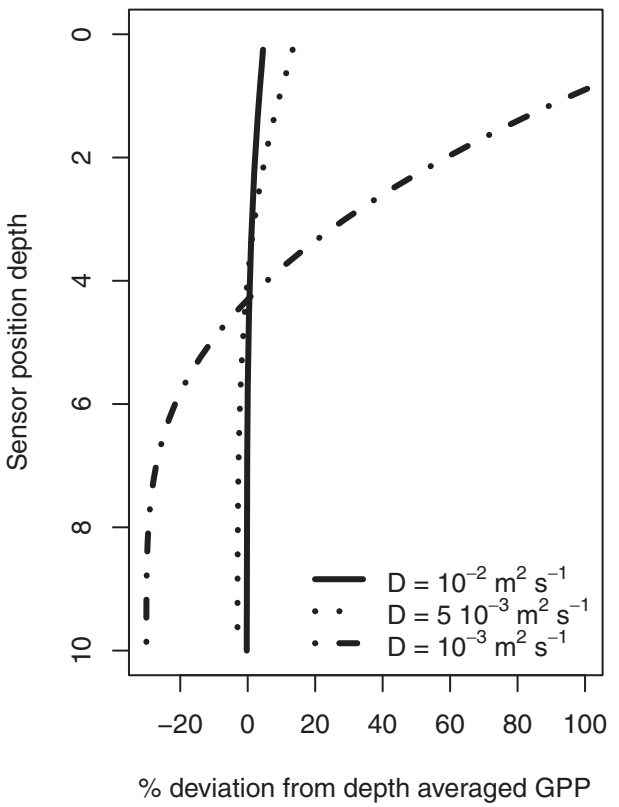

Fig. 4. Simulated depth profile of the relative difference of GPP estimates from single depth dissolved oxygen recordings. Simulations were performed with the vertical water column model with different turbulent diffusivities. To assure a high vertical gradient, the light attenuation coeffient was set te $k_d = 10\,m^{-1}$, piston velocity $k = 5\,m\ d^{-1}$ and incident irradiance was taken from the first two weeks of June.

signal is not dependent on the depth location of the sensor). Clearly, if one deploys a single sensor in a field situation, this sensor will not necessarily record the average oxygen concentration of the control volume. The degree to which the sensor signal will match the depth-averaged oxygen concentration will depend on the sensor's position in the water column, the vertical gradient in GPP and on the amount of turbulent mixing.

The water column model allows us to quantify this mismatch by applying the Fourier method to model output at different depths. This emulates the application of the Fourier method to the oxygen signal of a sensor fixed at those depths. Figure 4 shows the relative difference between true simulated GPP and the Fourier method estimate, for different turbulent diffusivities in a high vertical gradient situation (k_d=10 m^{-1}; k=5 $m\,d^{-1}$; light forcing first two weeks of June).

For all mixing intensities, the Fourier method overestimates depth averaged GPP when it is applied to oxygen concentrations from the upper water layer, while it underestimates GPP at deeper depths. However, the underestimation when the sensor is fixed deep in the water column is always lower than the overestimation when it is fixed at shallower depths. For strongly mixed systems ($D = 1 \times 10^{-2}\,m^2\,s^{-1}$), the vertical dependence of GPP estimates is very small, with less than 5% overestimation when the sensor is fixed in the upper meter of the water column, and less than 1% underestimation in the deepest part of the water column. For the weakly mixed system ($D = 5\times10^{-3}\ m^2\ s^{-1}$) the overestimation in the upper meter can be up to 15%, though it reduces quickly to below 5%, when the sensor is positioned below 2 m of water depth. The underestimation for deeper sesnor positionings reamins lower than 3%. When the mixing intensity is further decreased to $D = 10^{-3}\ m^2\ s^{-1}$ the mismatch becomes large, with an overestimation of over 100% in the upper meter, and an underestimation of almost 30% in the deepest parts. Note that this depth dependency of the GPP estimate is not specific for the Fourier method, but applies to all diel oxygen methods based on a zero-dimensional mass balance. Our results, hence, imply that a correct sensor positioning is crucial in diel oxygen methods based on single depth measurements, especially in weakly mixed systems. Alternatively, depth integrated O_2-concentrations could be calculated from simultaneous observations at different depths with a sensor array.

Estuarine model

The water column simulations indicate that many estuarine and coastal systems have a vertical mixing intensity that is large enough to assume that vertical mixing is instantaneous. In such systems, the oxygen dynamics can be realistically simulated with the one-dimensional estuarine model presented above. Figure 5 (top panel) shows the resampled output of that model, forced with observed irradiance from 6 June to 3 July and resampled with velocities from the same period. The major pattern in this time series is the tidal oscillation of the concentrations of both oxygen and algal biomass. This pattern is so strong that it almost completely masks the diel fluctuations caused by primary production. As a simple illustration of the power of the Fourier transform in separating the diurnal component of a signal from components with other periodicities, the bottom panel shows the Fourier amplitudes of the time series. In this figure, the diel fluctuations clearly show up as a peak at 1 cycle per day.

Figure 6 shows the time average of resampled gross primary production for all 14-d long simulations and the result of applying the Fourier method to the corresponding resampled oxygen time series. The overall correspondence is very good, but the bias is relatively large during months with low primary production, and a seasonal trend in the bias is apparent. In absolute terms, the bias ranges from about −26.2 to 23.7 mmol $O_2\ m^{-2}\ d^{-1}$. The average bias throughout the year was 0.6 mmol $O_2\ m^{-2}\ d^{-1}$, standard deviation 9.5 mmol $O_2\ m^{-2}\ d^{-1}$. During April to September (the months where GPP is highest), the average bias was

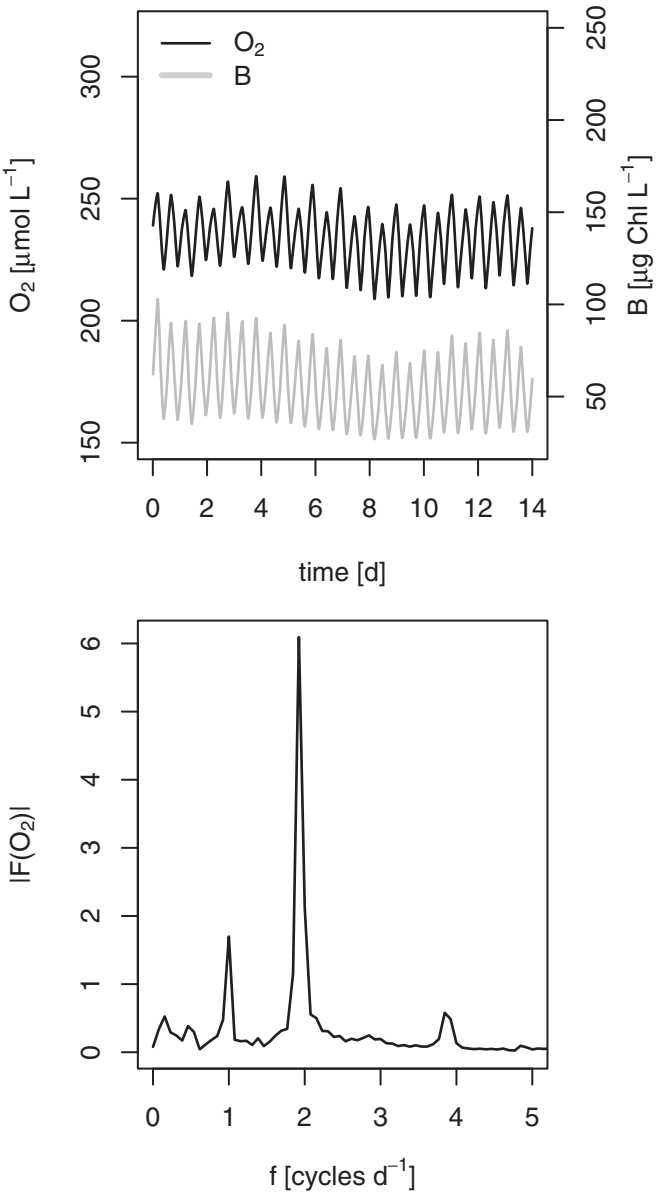

Fig. 5. Output of the estuarine model forced with observed irradiance from 6 June to 3 July and resampled with velocities from the same period (top). Fourier amplitudes of the oxygen time series (bottom).

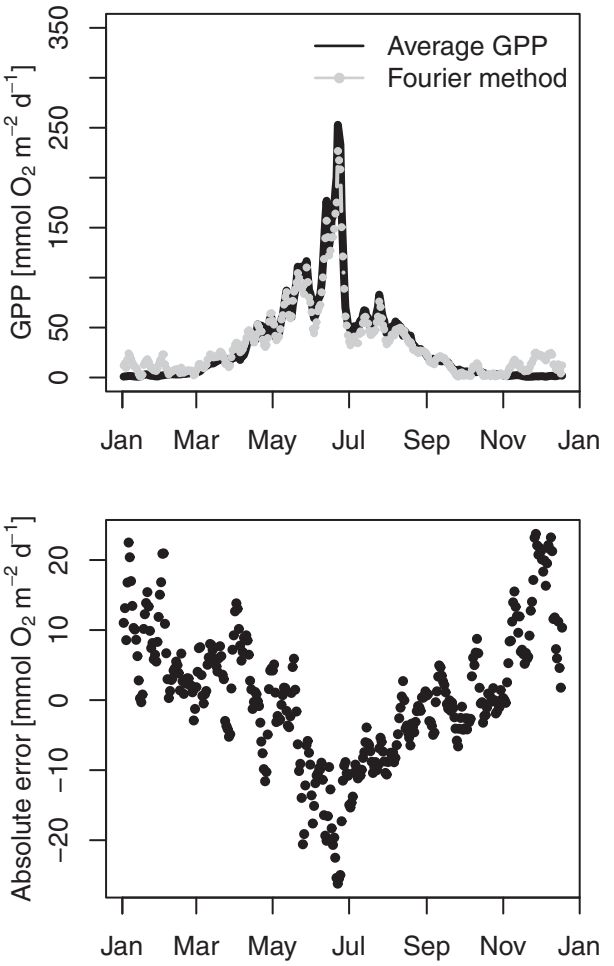

Fig. 6. Simulated GPP and Fourier method estimate, calculated from resampled estuarine model output for all subsets of 14 consecutive days of observed irradiance (top). Mismatch btween average GPP and Fourier estimate (bottom).

-5.1 mmol O_2 m^{-2} d^{-1}, standard deviation 7.7 mmol O_2 m^{-2} d^{-1}. In relative terms, the bias on the Fourier method calculated from all simulations from April to September is $-7.3 \pm 19.8\%$. Put differently, about 75% of GPP-estimates in April–September lie within a band of -25% to $+5\%$ of true average GPP. In winter months, when production is low, the diurnal fluctuations induced by primary production are sometimes orders of magnitude lower than the ones induced by other simulated processes or artefacts induced by signal processing.

From the resampled GPP time series, we can compare the truncated sinusoid approximation with the time average of resampled GPP. The truncated sinusoid approximation overestimates GPP by 0.3 ± 0.7 mmol O_2 m^{-2} d^{-1}, or in relative terms $1.7 \pm 1.2\%$.

The bias of the Fourier-based GPP estimate largely results from the effect of the horizontal advective fluxes induced by the tides. Indeed when calculated in the reference frame moving with the tides, the absolute error from April to September is only 0.5 ± 1.4 mmol O_2 m^{-2} d^{-1}. From the model output, we can easily calculate the Fourier amplitude of the advective transport term, and, therefore, its effect on the Fourier amplitude of the oxygen signal. If we correct for this contribution, the absolute error from April to September is reduced to 1.2 ± 1.4 mmol m^{-2} d^{-1}, demonstrating that the error originates from the advective fluxes rather than dispersive fluxes, other processes or signal processing artefacts.

At this point, it is instructive to compare the Fourier method with a classic bookkeeping approach, senso Cole et al. (2000). Figure 7 shows the correlation between

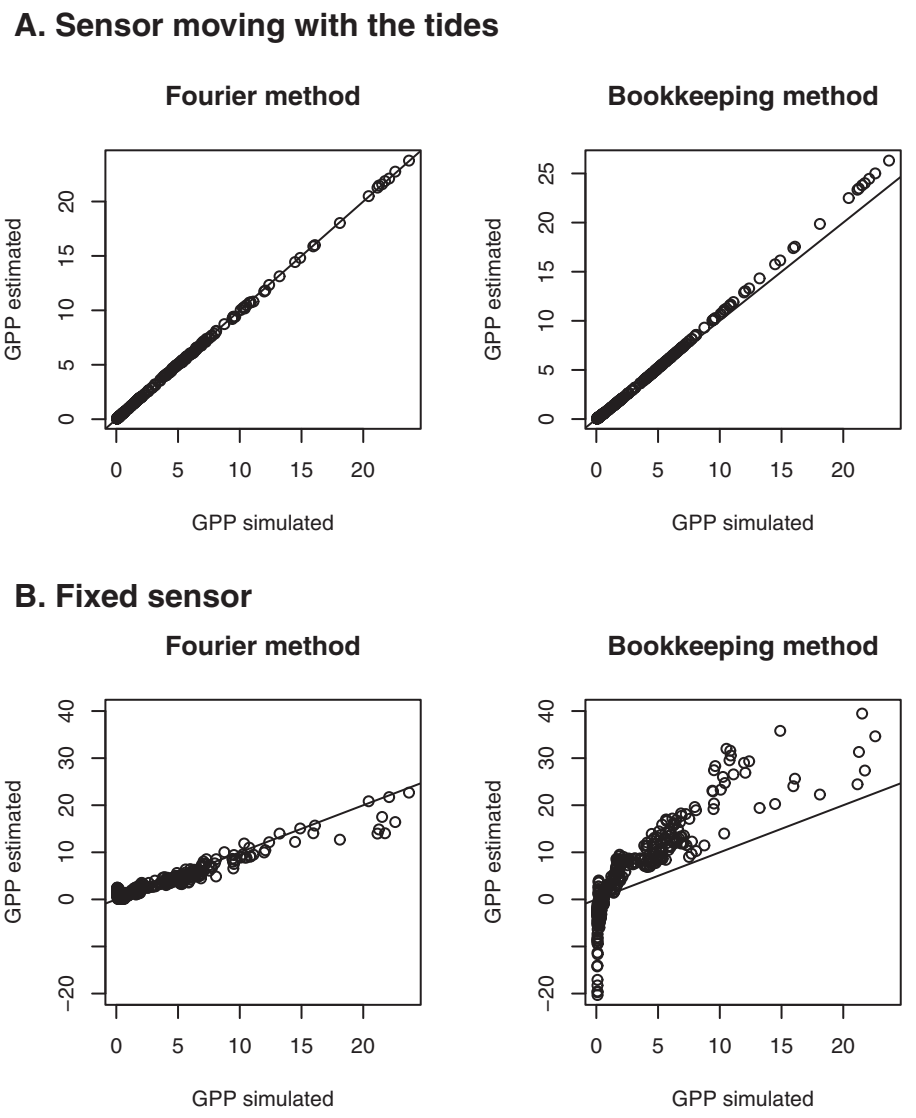

Fig. 7. Comparison of the Fourier method with the bookkeeping method applied to simulated O_2-series in the moving reference frame (top) and in the fixed reference frame (bottom). Lines have slope = 1 and intercept = 0.

simulated GPP and GPP estimated with the Fourier method (left) and the bookkeeping approach (right). The piston velocity was assumed to be known exactly in the bookkeeping approach. The top panels show the results when both methods are applied to O_2 time series obtained in the moving reference frame, as if the sensor would follow the tides perfectly. Slope and intercept are, respectively, 1.0 and 0.1 for the Fourier method ($r^2 > 0.99$) and 1.1 and − 0.1 for the bookkeeping method ($r^2 > 0.99$). Apparently, with the current simulation settings, the bookeeping method overestimates true GPP. The bookkeeping method does not account for horizontal turbulent fluxes and for oxygen demand processes, therefore, it is not surprising that it misses GPP, even though air–water exchange was assumed to be perfectly known. The bottom panels show the results when both methods are applied in a fixed reference frame. There, the bookkeeping method goes completely wrong. This is not surprising, since no correction for advective fluxes has been performed at all. However, such correction has neither been applied for the Fourier method. The left pane presents the same results as Fig. 6, but now as a correlation plot between simulated and estimated GPP. Slope and intercept are respectively 0.8 and 0.7 (r^2=0.94).

Field data

At the field sampling location, the oxygen concentration shows a strong gradient along the estuary axis. Therefore, the dominant periodicity in the field data oxygen time series results from the tidal movement of water masses. Figure 8a,c. show typical 14-d excerpts of recorded oxygen

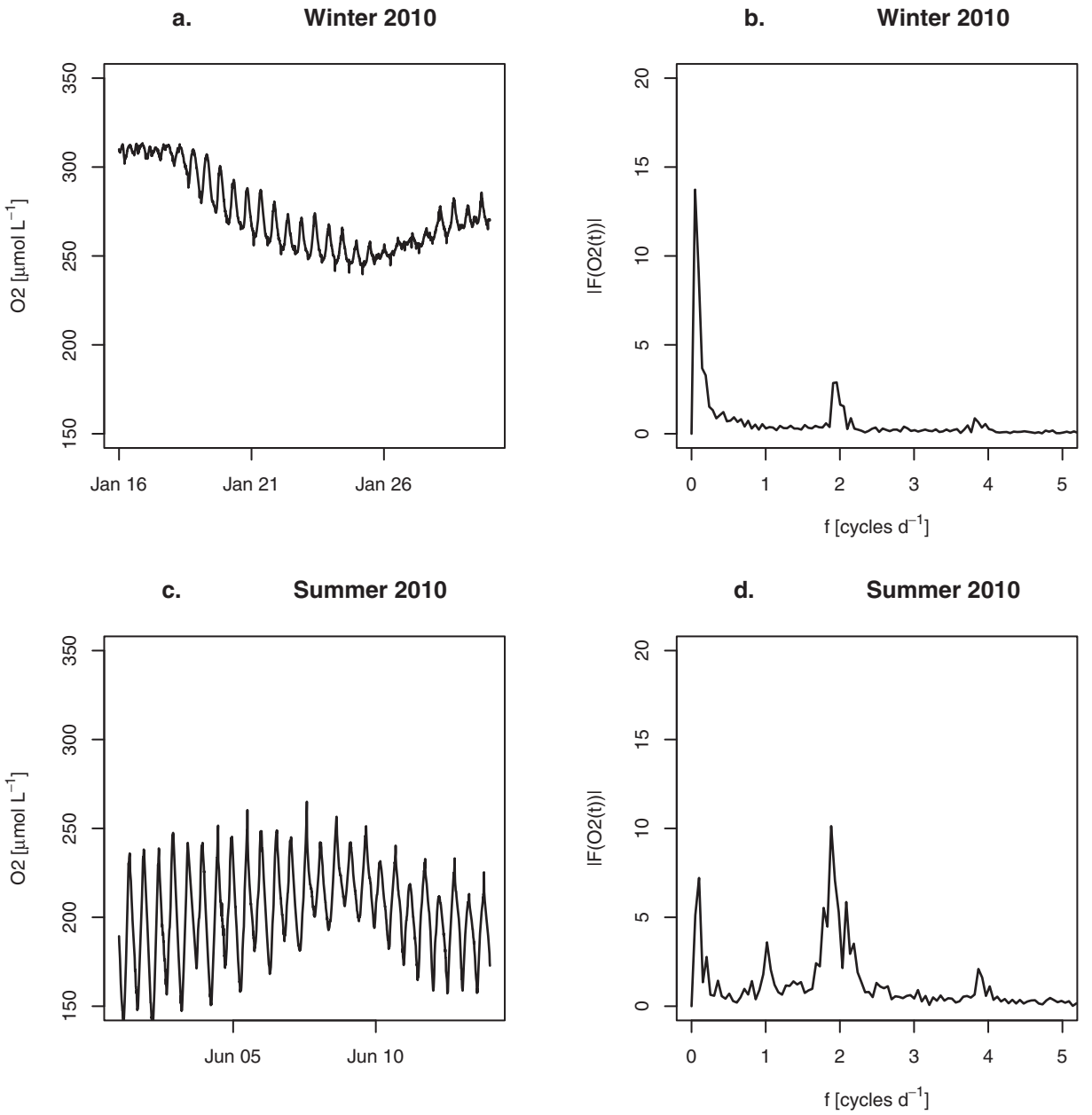

Fig. 8. Typical 14-day excerpts of dissolved oxygen time series in Winter and Summer. Oscillations in the time domain (a. and c.) show up as peaks in the frequency domain (b. and d).

concentrations in winter and summer periods. The most prominent periodic constituent of the tides is the semi-diurnal M_2 component with a period of 12 h 25 m. This M_2 component is directly observed in the oxygen signal. Note that in winter, the amplitude of the tidal oscillation in the O_2 concentration is much smaller than in summer, due to the smaller longitudinal gradient of oxygen in winter.

The associated Fourier transforms of these winter and summer time series are shown in Figure 8b,d. The tidal oscillations show up as marked peaks at a frequency of slightly less than two cycles per day. The peak at low frequencies (0–0.5 cycles per day) results from longer-term trends in the oxygen signal. The main difference between both Fourier transforms is the appearance of a peak at 1 cycle per day in the summer series, resulting from primary production. In the time domain graphs (Fig. 8c), this effect of primary production is hard to distinguish by visual inspection, while in the Fourier transform (Fig. 8d) it is readily apparent.

Note that the Fourier transform of the summer time series is comparable to the transform of the estuarine model

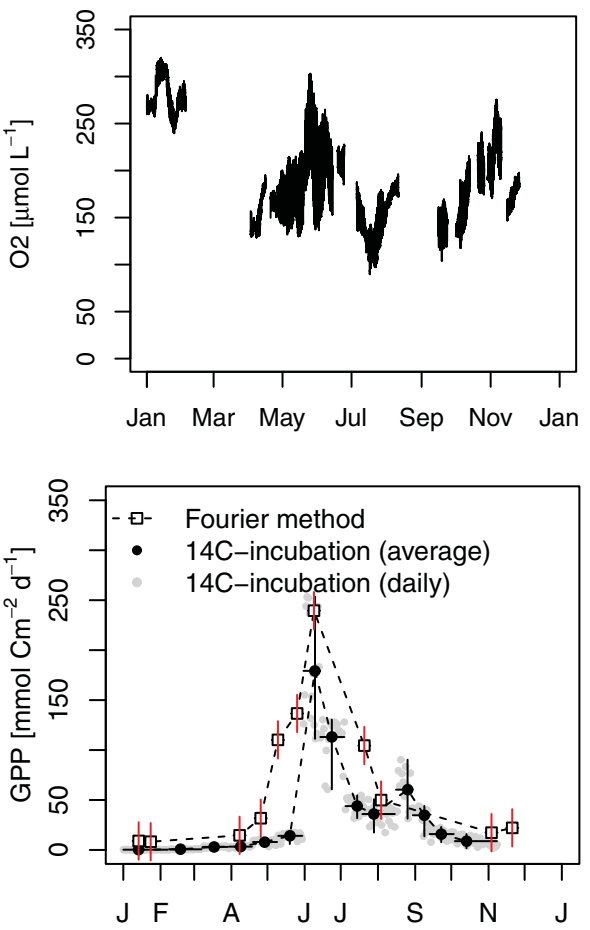

Fig. 9. Dissolved oxygen data (top) and comparison of the Fourier method estimate of daily primary production rates (GPP) and results from ^{14}C incubation (bottom). Horizontal bars on Fourier method estimates represent the length of the dissolved oxygen time series used. Vertical bars are estimated standard deviation of the effect of diurnal components in the tides, based on observed gradients. Black dots represent the days on which photosynthetic parameters were determined with the ^{14}C method. Horizontal bars on ^{14}C-based GPP estimate represent the time range on which observed photosynthetic parameters were used to calculate GPP (^{14}C-based estimate). Vertical bars represent the variability in the ^{14}C-based estimates within this time range, due to incident light variability.

output presented in Fig. 5. The similarity of the magnitude of the semi-diurnal peak indicates that the simulated horizontal gradient in oxygen concentration is representative for the field situation. For its part, the similarity of the diurnal peak indicates that simulated gross primary production is also comparable to the field situation.

Figure 9 shows all available oxygen time series in 2010 at the study site (top panel), and the comparison of Fourier method based and ^{14}C-based GPP estimates (bottom panel). The volume-specific Fourier-estimate of GPP was converted to area-specific GPP by multiplying with the average water depth near the field station (9.2 m). A photosynthetic qoefficient (PQ) of 1.3 was used to convert the oxygen based GPP values to carbon units, corresponding to the theoretical PQ when carbohydrate production uses nitrate as a nitrogen source (Williams et al. 1979; Gazeau et al. 2007). A point by point comparison of the two methods is not possible since the sampling periods do not match exactly. But overall, GPP estimates with the Fourier method and from ^{14}C incubations are in the same order of magnitude and display the same seasonality. However, GPP estimated with the Fourier method is consistently larger than estimates from ^{14}C incubations. The highest discrepancy is observed in Spring 2010 (April–May observations).

As outlined in the methods section, an estimate of the magnitude of the bias resulting from the diel component of the tides can be obtained from combining continuous salinity data with observed salinity and oxygen profiles along the estuarine gradient. We calculated the bias on the 11 continuous time series of more than 10 d, amounting on average − 4.4 mmol C m^{-2} d^{-1}, with standard deviation 15.6 mmol C m^{-2} d^{-1}. The full range of bias was − 43 to 9.5 mmol C m^{-2} d^{-1}. There was no seasonality. These estimates are in the same order of magnitude as the estuarine simulation results. These results are rough estimates of the effect of the tides. Therefore, we did not correct the Fourier estimates with the estimated bias, but we did add indicative error bars on the Fourier estimates in Fig. 9. These error bars were set equal to the observed standard deviation (15.6 mmol C m^{-2} d^{-1}).

Both daily and averaged ^{14}C-based GPP estimates are shown in Fig. 9. The daily production data appear as distinguished clouds on the plot. This illustrates the effect of assuming that factors such as k_d, Chl *a*, and photosynthetic parameters do not change during the interval for which the average is calculated (based on observed irradiance data).

Discussion

Comparison of Fourier method and ^{14}C incubation

Compared to bottle methods, diel oxygen methods generally result in higher GPP estimates (Kemp and Boynton 1980; Swaney et al.1999). This discrepancy is attributed to limitations of bottle incubation methods. Swaney et al. (1999) list as main limitations of bottle methods: reduced turbulence, unnatural light fields, respiration of ^{14}C-labeled organic matter, and altered grazer communities. These problems may be particularly intense in turbid and deeply mixed estuaries: for example, Kemp and Boynton (1980) found that GPP estimates from bottle methods in Chesapeake Bay were a factor 1.5–4 lower than values obtained from diel oxygen method. Westberry et al. (2012) found that bottle methods consistently underestimated photosynthesis by 20–40% in oligotrophic oceans. After a detailed analysis of the potential explanations, they concluded that the exact physiological nature of the underestimate was yet to be demonstrated. Note that in our case study, benthic production is negligible

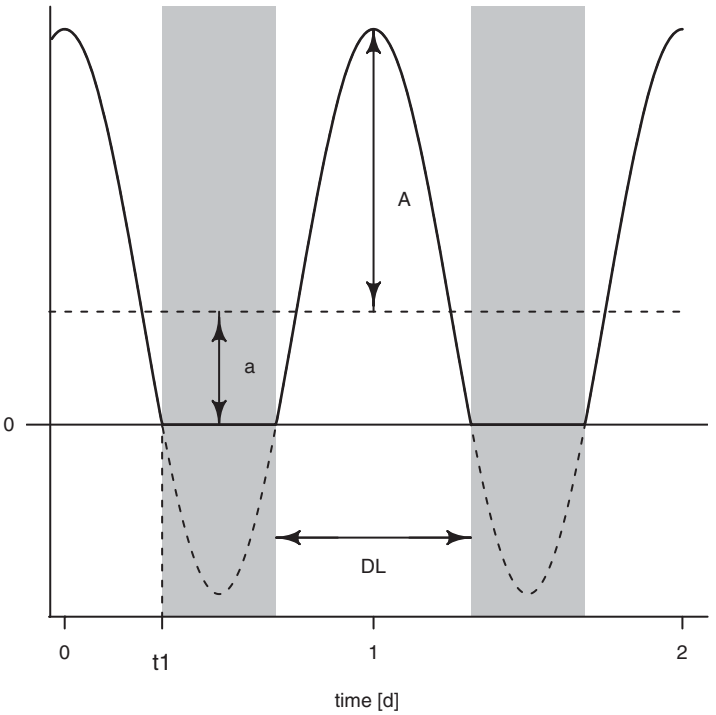

Fig. 10. When gross production is assumed a truncated sinusoid $GPP(t) = \max(0, a+b\cos(\omega t))$, the parameters a and b are related to the relative fraction of light hours during the day ($f_{DL} = DL/24h$). From the figure: the number of daylight hours $DL = 2t_1$, with $b\cos(\omega t_1)+a=0$. Therefore, $\pi f_{DL} = \cos^{-1}(-a/b)$.

compared to pelagic production, both due to high turbidity levels and the small area of tidal flats (steep slopes due to embankments). However, in systems where benthic production is significant and not accounted for, benthic production would also contribute to the mismatch between ^{14}C and diel oxygen methods.

GPP estimates also vary substantially between different bottle methods. Gazeau et al. (2007) compared three different incubation methods to estimate GPP in the Scheldt estuary: the oxygen light-dark method (O_2-LD), ^{14}C incorporation and ^{18}O labeling. They concluded that the O_2-LD technique is expected to give higher rates than the ^{14}C method mainly because of (1) possible respiration of ^{14}C labeled organic matter in the cell to an extent that depends on incubation time, (2) stoichiometric relationships between O_2 and CO_2 (PQ) (which depends on the nature of the nitrogen substrate and of the organic carbon product), and (3) possible excretion of $DO^{14}C$. In the Scheldt estuary they observed an increase in the ratio between O_2-LD and ^{14}C GPP-estimates with decreasing salinity. Remarkably, at their most upstream station, which is less than 10 km from our study site, this ratio was about 6.

Another major source of uncertainty impinging on ^{14}C-based GPP estimates is the need for an estimate of the light attenuation coefficient k_d. In the turbid Scheldt estuary, k_d is known to be a highly variable parameter with both within day and day to day variability (Desmit et al. 2005). A point measurement of k_d, which is commonly used for calculation of depth integrated production (Kromkamp and Peene 2005), is not reliable. Therfore, we calculated depth integrated production with a typical value of $k_d = 4.5 m^{-1}$. For sure, this will underestimate light availability during some periods, while overestimating it for others. At this study site, the only reliable option to account for the real light availability would be to continuously measure k_d, for example, making use of two PAR-sensors seperated by a known distance.

Algal biomass (Chl *a*) and photosynthetic parameters (α, P_m) are assumed constant between measurements of photosynthetic parameters (typically 2 weeks to 1 month). This explains the jumps between clouds of day-to-day GPP estimates (Fig. 9). Linearly interpolation of these parameters between consecutive sampling times could improve the GPP estimate, altough still this would be an approximation. Finally, the calculation of depth integrated production from bottle methods requires a fair amount of data manipulation (depth integration, time interpolation), with data from different sources (incident irradiance, Chl *a*, light attenuation, photosynthetic parameters, channel bathymetry). As any of those data can only be determined with a certain accuracy, such data manipulation easily leads to uncertainty accumulation.

Like other diel oxygen methods, the Fourier method is not plagued by the variability in k_d or other parameters, nor does it need to be integrated over depth. On the contrary: it is based on oxygen concentrations which inherently integrate the gross primary production over the real light field, biomass and photosynthetic parameters and, when mixing is fast enough, over the water column. From the field dataset, we conclude that the Fourier method estimate of GPP is in the same order of magnitude and displays the same seasonality as the results from the bottle incubation. The difference between both methods is in line with results from other studies that compare in situ with bottle methods and with the performance of ^{14}C incubations at the study site.

Accuracy of the Fourier method in estuarine systems

Our analysis of the performance of the Fourier method on synthetic O_2-series sheds light on the accuracy of the Fourier method and the validity of its assumptions at the study site. For turbid estuarine systems ($k > 2\ m^{-1}$), where the light saturation parameter is typically $E_m = 250 \mu mol\ photons\ m^{-2}s^{-1}$, the difference between the truncated sinusoid approximation and true GPP calculated with the idealized pond model was 3±4%. Interestingly, this difference decreases when biomass was dynamically simulated, both in the open water model and the estuary model. There the difference was 2.6± 2.8% and 1.6±1.2%, respectively. Thus, in an estuarine or coastal setting the simulation results indicate that the

truncated sinusoid approximation leads to a slightly upward biassed GPP estimate (1.7% to 3%), with a random error of 1.2 to 4%.

This upward bias is partly offset by the downward bias introduced by neglecting diurnal fluctuations in air–water exchange. Simulation results from the open water model indicate that with a water depth of 10 m, and a typical estuarine vertical mixing coefficient of 10^{-2} m^2s^{-1}, the maximal error made by neglecting this damping is small (1.4%). This can be considered an upper limit as it was obtained by setting the light attenuation coefficient to a large value of $10\,m^{-1}$, and choosing the period with highest incident irradiance. Still, although this simulation was done with a finite mixing rate, this assumes that we can observe the true depth averaged oxygen concentration. At the field location oxygen was recorded at a constant depth of 0.75 m. At this depth, the open water model simulates 3.8% to 11.8% overestimation when vertical turbulent diffusivities decrease from 10^{-2} to 5.10^{-3} m^2s^{-1}. Tidal currents are very high at the field location, with maximal currents during a tidal cycle often 1.2 m s^{-1} or more. Consequently, the vertical mixing coefficient at the field location often be larger than 10^{-2} m^2s^{-1}. This, combined with parameter values that assure maximal gradients, suggests that the simulated 3.8% overestimation in the open water model set an upper limit on the bias due to air–water exchange.

Thus, it seems that at our Scheldt estuary field site, the largest source of error results from from diurnal fluctuations in horizontal fluxes. Both the estuarine model simulations as the observations-based error estimate indicate a slight downward bias: − 5.7 mmol O_2 m^{-2} d^{-1} based on observations, and 0.6 (full year average) to − 5.1 (April–September average) mmol O_2 m^{-2} d^{-1} based on the simulations. Standard deviation is 20.3, 9.5, and 7.7 mmol O_2 m^{-2} d^{-1}, respectively. This means, among others, that the Fourier method when applied to the study site will be inaccurate in Autumn and Winter months when production is expected to be of the same order or less than the effect of diurnal fluctiations in horizontal fluxes.

Our simulations also shed some light on the sources of the diurnal fluctuations in horizontal fluxes. A priori, we anticipated that a horizontal gradient in GPP causing a diurnal changing horizontal gradient in O_2 concentrations would lead to diurnal pattern in horizontal dispersive flux. However, the simulation results indicate that this effect is a factor 10 lower than the effect of diurnal fluxes in advective fluxes: the error on the GPP estimate in the moving reference frame was only 0.5 ± 1.4 mmol O_2 m^{-2} d^{-1} compared to -5.1 ± 7.7 mmol O_2 m^{-2} d^{-1} in the moving reference frame. For its part, the diurnal fluctuations in advective fluxes can have two origins: they can be true diurnal harmonics of the tide, or they can result from leakage of other harmonics. The two most important tidal harmonics with close to diurnal frequency are the K_1 and O_1 lunar diurnals with respective period of about 23.9 h and 25.8 h. Neither of them correspond to Fourier frequencies in times series of 14 d and a 10 min sampling interval. Therefore, although their amplitudes are relatively low (about 3% and 5% of the semi-diurnal M_1 near the study site) their presence will certainly leak into the closeby diurnal Fourier frequency. On the contrary, the semi-diurnal M_1-component of the tide is located much farther away, but the estimate of the diurnal amplitude could still be affected by leakage due to the large amplitude of M_1. The magnitude the diel fluctuations in advective fluxes depend both on the horizontal gradient in oxygen concentration and on the relative magnitude of the tidal harmonics, both of which are system dependent. Therefore, the bias and error calculated with the estuary model are indicative for the case study site, but cannot be generally applied to other systems.

There are two common approaches to reduce the effect of leakage: removing the components that cause the leakage and tapering (Bloomfield 2000). Since the frequencies of tidal harmonics are well-known we anticipate that the first approach could result in an improvement of the Fourier method in estuarine and coastal systems. The second approach, tapering, has a more complicated effect. Indeed, athough it is an elegant leakage reduction strategy, the Fourier method averages GPP over the length of the O_2 time series, and tapering the series would favour daily cycles in the middle of the series over those at the end. Thus, it should be carefully examined how it affects the time interval for which the Fourier estimate is representative.

As a side remark: we have chosen to answer pragmatic questions with our simulation studies: How good does the Fourier method perform when O2 time series of 14 d are available? What is the impact of seasonality on this performance? This motivated our choice for running 14-d windows. We have restricted ourselves to the quantification of standard error and relative error (both full year and May–September estimates for the estuarine simulations), and a visualisation of residuals to indicate seasonality and give an idea of the stationarity of variance of these residuals. Obviously, there is considerable autocorrelation in consecutive 14-d averages of GPP, and a similar autocorrelation would be found in correct estimates of GPP. As a result, it is likely that the difference between real GPP and the Fourier estimate of GPP has more structure (e.g., autocorrelation) than what is presented in the manuscript. The full analysis of this error structure and also of the impact of leakage reduction on the accuracy of the Fourier method is beyond the scope of the current manuscript.

Combined, for conditions at the field side, the upward biases of the truncated sinusoid assumption and of the single depth measurements, and the downward biases of neglecting air–water exchange and neglecting the advective fluxes cancel out to a large extent. Neglecting diel fluctuations in advective tidal fluxes is by far the largest source of random

error on the Fourier estimate. The simulations indicate that the error on the method is relatively small. Given the inherent limitations of ^{14}C-incubations, in particular the effect of high $DO^{14}C$ production and of the highly variable light attenuation in turbid Scheldt estuary, this suggests that at the study site the Fourier method gives a more accurate estimate of GPP than the bottle incubations.

Stochastic drivers and observational error

The simulations were aimed at investigating the effect of the simplifying assumptions on the GPP estimate. By choosing appropriate parameter settings, we could evaluate the validity of the assumptions in different environmental settings. This resulted in valuable insight in the applicability of the method in a range of aquatic systems (*see* also below). This approach does not account for the impact of stochastic drivers and observational error on the method's accuracy, but we can use some theoretical results to assess them. First, the presence of a random error without autocorrelation and with variance σ^2 on the O_2 observations will be spread over all frequencies and, hence, also the diurnal frequency. The resulting estimates of the Fourier amplitudes are unbiassed, and their variance is given by $2\sigma^2/n$, with n the number of data points (Bloomfield 2000). Taking the square root of the variance as the typical difference between true and observed A_{O_2} we can estimate the corresponding error on the estimate of GPP with Eq. 5. We can compare this with the simulation results of Batt and Carpenter (2012) who investigated the accuracy of different diel oxygen methods in the presence of stochastic drivers and observational noise. They simulated the effect of observational noise with variance 1 to 500 $(mmolO_2\ m^{-3})^2$ on simulated 6 d long O_2-series with a time step of 4 minutes ($n = 2160$), generated with a model that was forced with observed PAR from May 2010. We calculated the relative fraction of daylight for this time period as fDL = 0.67 (Anonymous 2011). Substituting the square root of the expected variance on the Fourier amplitude into Eq. 5, the typical difference between true GPP and observed GPP amounts to 0.3-6.5 $mmolO_2\ m^{-3}\ d^{-1}$. These values are very similar to the values that Batt and Carpenter (2012) obtained using a Kalman filter to estimate GPP suggesting that the Fourier method performs equally well in the presence of observational noise. This contrasts to their results with the bookkeeping method applied to unfiltered O_2-series which is much more sensitive to observational noise. However, this does not surprise us as differencing is a high pass filter. Thus, low-pass filtering the raw O_2 time series before calculating differences for the bookkeeping method amounts to common good practice.

By shifting the focus to the frequency domain we also gain some useful insights on the effect of stochastic drivers of O_2 dynamics. The derivation of the Fourier method and the simulation we performed assumed only deterministic processes in the O_2 dynamics. However, the central Eq. 5 also applies when the power of nondeterministic (or stochastic) process influencing O_2 dynamics in the vicinity of the diurnal frequency can be assumed negligible. This assumption is not trivial, as any process with a continuous spectrum would have power in all frequencies, and, thus, also the diurnal frequency. This effect is not restricted to the Fourier method: indeed stochastic processes with power around the diel frequency would affect any instance of the diel oxygen method. It is difficult, and without any further assusmptions impossible, to filter out its effect on the metabolic estimate. This is nicely illustrated by Batt and Carpenter (2012) for the simplest form of stochastically driven O_2-dynamics, that is, a random process error term added to the discretized verion of 5. This is equivalent to the addition of a random walk or Brownian noise to the O_2 time series. The power spectrum for Brownian noise is known to equal $\sigma^2/(n\omega^2)$, with σ^2 the variance of the random process error. We can estimate the typical effect of the presence of random process error to the estimate of A_{O_2} as the square root of this power spectrum evaluated at the diurnal frequency. On substitution in Eq. 5, we have an estimate of the typical difference between true and observed GPP, similar as with the observational error above. Doing this for variances applied by Batt and Carpenter (2012) (0.1, 0.5, 1, 5, 50 and 100 $mmolO_2\ m^{-3}$), the calculated typical differences amount to 3.7, 8.3, 11.7, 26.2, 82.9 and 117.3 $mmolO_2\ m^{-3}\ d^{-1}$. This very close to their simulated difference for the bookkeeping method (Fig. 2 in their manuscript). As Batt and Carpenter (2012) illustrate, it is almost impossible to filter out the contribution of process error to the diurnal frequency: even when assuming the exact model by which the data was generated, the linear model and Kalman filter estimates of GPP improved only marginally. In this respect the Fourier method does not perform better or worse than other diel oxygen methods, just as it does not resolve the problem of other deterministic processes with diurnal fluctuations, for example, community respiration.

Note that the observational error does not occur in our consideration in the frequency domain. Thus, we not only correctly explain the expected error on the GPP estimate introduced by a random process error, this also explains why it is invariant under changes of the observational error [*see* figs. 2–4 of Batt and Carpenter (2012)]. This result clearly demonstrates the power of shifting the attention towards the frequency domain. A full treatment of how other nondeterministic drivers of O_2-dynamics affect diel oxygen methods is out of the scope of this manuscript, but we believe that further analysis will contribute to a increased understanding of how the different scales of the deterministic and nondeterministic parts of O_2-dynamics affect estimates of metabolism. This is a topic that has not received a lot of attention [*see*, however, Langman et al. (2010); Coloso et al. (2011)].

Model error

The assessment of bias and error of the Fourier method we provided, is based on synthetic oxygen data. Thus, strictly speaking, the presented results on bias and error are specific to the models that were used to generate the O_2-series, and, thus, to those real-world systems that are adequately represented by them. Every inverse modeling problem (and, thus, every flavour of the diel oxygen method) is affected to a certain extent by such model error (i.e., the uncertainty associated by the choice of mathematical formulation). It is important to note that the Fourier method is not dependent on the choice of models we used to generate synthetic oxygen data. Rather, apart from the assumption that only GPP causes diurnal fluctuations in O_2, the critical mathematical assumption of the Fourier method is truncated sinusoid approximation for the relation between time averaged GPP and its diurnal amplitude over the same period. This is a less critical assumption than made by all other inverse methods: although almost never explicitely acknowledged (Hanson et al. (2008) providing a notable exception), such inverse methods implicitely assume that the real world behaves normally around a predetermined set of equations. A detailed investigation of the effect of different model formulations on the assessment of the accuracy of the Fourier method is also beyond the scope of this manuscript.

Applicability of the Fourier method to other aquatic systems

Although the biogeochemical models inherently represent an idealization of reality, we can draw some general conclusions from the simulations. The results obtained with different parameterizations of the idealized pond model indicate that for many real-world systems the truncated sinusoid approximation is a robust assumption. In particular, in systems with the light extinction $k_d \geq 1$ and light saturation parameter $E_m \geq 100$, the GPP-estimate will be biased by at most 5% and the random error on a 14 d period will be of the same order of magnitude (Table 3). Conversely, the bias and error is largest when $k_d \leq 1$ or $E_m \leq 100$. These conditions are typical for many clear lakes and the open ocean. In those systems the truncated sinusoid assumption introduces a downward bias of up to 13% and an error of 9%. Photosynthesis in those systems is saturated over a (large) part of the water column for a (large) part of the day and, thus, the time evolution of GPP over a day will not behave as a truncated sinusoid. A similar situation will occur in nutrient limited systems where the maximal rate of production in a (large) part of the water column is determined by the rate of nutrient input and regeneration rather than by light availability. It could be possible in both light saturated and nutrient limited systems to find an alternative to the truncated sinusoid that better fits the evulotion of GPP over a day, and derive a more appropriate relation between A_{GPP} and time averaged GPP. However, this would involve further assumptions, to be evaluated case by case.

The open water model simulations indicate that the dampening of diurnal fluctuations in depth averaged O_2 concentration due to air–water exchange are often small. With a vertical turbulent diffusivity $D \geq 5.10^{-3}$, light attenuation coefficient k_d=10 m^{-1} and piston velocities ranging from 0.5 to 5 m d^{-1}, the bias introduced by neglecting air–water exchange correction is 0.2–3.8%(Table 4). These simulation settings are typical for maximal vertical gradients in turbid estuarine and coastal environments where tidal currents and overlying winds induce strong mixing and high piston velocities. The clear water simulations ($k_d \leq 1$ m^{-1}) indicate that with a piston velocity of 0.5 m d^{-1} and turbulent diffusivities as low as 10^{-6} m^2 s^{-1}, the underestimation of GPP due to neglecting air–water exchange is only 0.75%. Thus, also in clear lakes and the open ocean the dampening due to air–water exchange will often be negligible, resulting in a downward bias of the GPP estimate of only a few percent. Note that all simulations assumed a water colum of 10m depth. In shallower systems, the impact of neglecting air–water exchange will be larger, in deeper systems it will be smaller.

The above analysis of the truncated sinusoid assumption and of the effect of air–water exchange assumed that the depth averaged O_2 concentration is known. When depth gradients persist due to stratification, the assumption of instantaneous mixing is violated, and, thus, the Fourier method, as any other diel oxygen method, will underestimate total GPP when applied to epilimnion O_2 time series only. In such cases, depth averaged GPP can be readily estimated with the Fourier method by applying it to the depth averaged O_2 concentration calculated from a sensor array. Our model simulations show that also in water columns with a more simple vertical structure (a constant turbulent diffusivity throughout the water column), a correct positioning of sensors is crucial and a multisensor approach might be preferable. The simulations with intermediate mixing rates (D=5 $10^{-3}m^2s^{-1}$) suggest that the Fourier method can overestimate true GPP with up to 15% when applied to oxygen data from the upper meter of the water column. In the lower part of the water column, the Fourier method underestimates true GPP, but the difference is smaller. The effect of vertical mixing and air–water exchange need careful examination in every new environment where the Fourier method is to be applied. Without prior knowledge of the mixing properties, and without the possibility of deploying a sensor array, a good approach would be to put the sensor halfway the mixed layer depth.

Alternatively, both in the case of horizontal or vertical gradients, one could try to estimate the transport associated with the observed gradients [e.g., Kemp and Boynton (1980)]. Also when GPP estimates at different depth are derived from a sensor array, the fluxes between adjacent

water layers need to be estimated, for example, from observed vertical O_2 gradients. This requires an estimate of the turbulent diffusivity or other assumptions about the transport in the system. Estimating gradients from concentration differences magnifies error on the observations (differencing is a high pass filter). Because of the extra assumptions needed to constrain those fluxes, and due to the amplification of observation error, the deduced biological rates are prone to large error. In relatively stable lake systems these errors might not be prohibitive and indeed this approach is often used [e.g., Sadro et al. (2011); Obrador et al. (2014)]. But particularly in estuarine and coastal systems it is not recommended (Kemp and Boynton 1980). In the frequency domain this problem is again one of estimating diurnal fluctuations, but now in the vertical fluxes between different water layers. Estimating those fluctuations cannot be done without further assumptions about mixing processes. In this respect the Fourier method would not perform better or worse than any other diel oxygen method when vertical gradients are present. But how this could be done in the frequency domain is not a trivial question: additional mathematical treatment in the frequency domain is needed to assess whether and how the Fourier method can be adapted and whether it would perform better or worse than multisensor approaches in the time-domain.

Even more difficult would be the mathematical treatment in the presence of horizontal gradients in a 2D setting. Indeed, Van de Bogert et al. (2012) convincingly demonstrated that the assumption of horizontal homogeniety is often not met in lake ecosystems. Based on two case studies they found that single sensor derived GPP estimates varied over more than an order of magnitude between different locations. As made explicit in the theoretical derivation of the method, its application on single sensor data would yield a GPP estimate specific for a certain control volume around the sensor, and only in the absence of diurnal fluctuations in the fluxes through the boundaries of that volume. The latter assumption is violated in systems with finite mixing between regions with different productivity. Implicitely, however, this assumption was made by Van de Bogert et al. (2012). Since they did not account for fluxes between locations, they probably underestimated GPP at the highest productive sites and overestimated GPP at the lowest productive site. In order for the Fourier method to give reliable whole system GPP estimates in the presence of this type of horizontal variability, the method could be applied to a system-averaged O_2 time-series (This is entirely similar to the situation whith vertical gradients).

In estuaries and coastal systems with strong horizontal gradients and advective fluxes related to the tides, we have demonstrated the merits of the Fourier method. Particularly in those systems, the in situ diel oxygen method is prone to large error. Therefore, they are among the systems where the practical advantages of bottle methods outweigh their limitations, and are still often used for estimating GPP and ecosystem metabolism (Gazeau et al. 2007). The workaround proposed by Swaney et al. (1999) is based on intensive sampling cruises along a transect (4 cruises spread over 2 d for each production estimate), and is based on a first order approximation that estimates GPP from a linear regression of oxygen against salinity, depth and time. Also, a correction for air–water exchange was needed. Vallino et al. (2005) used a method based on assimilation of dissolved oxygen data in a full transport-reaction model. But also there, spatially distributed dissolved oxygen data is necessary and the resulting GPP estimates strongly depend on the reliability of other components of the model. Two major reasons make diel oxygen methods difficult to apply in estuarine and coastal systems: 1. the tidal signal dominates O_2 time series and 2. gas transfer is high and difficult to correctly estimate. Based on the simulation results and the case study, we conclude that the Fourier method circumvents these problems to a large extent. Importantly, our simulation results indicate that the large vertical mixing intensities, large light attenuation and high light saturation parameter typical for estuarine and coastal phytoplankton communities make estuaries and coastal systems particularly suited for application of the Fourier approach. This makes the method a new and powerful tool for estimating GPP in estuarine and coastal systems, and as such enlarges the number of systems where GPP can be estimated from in situ oxygen concentrations. This is particularly relevant at a time when deployment of continuous measurement devices is on the rise in a diversity of aquatic systems. In systems where the method give appropriate results, it has the potential for automation and for real-time and quasi-continuous observation of GPP. With its reliance on just one data-source and clear data processing procedure the method is a major contribution to GPP estimation.

APPENDIX

Characteristics of the truncated sinusoid

Consider the truncated sinusoid (Fig. 10)

$$f(t)=\max(0, a+b\cos(\omega_1 t)) \tag{14}$$

This is a periodic function with period $T=2\pi/\omega_1$. The average value of this function is calculated as

$$\frac{1}{T}\int_0^T f(t)dt = \frac{b}{\pi}(\sin(\theta)-\theta\cos(\theta)) \tag{15}$$

$$\text{with} \quad \theta = \cos^{-1}(-a/b) \tag{16}$$

Like any periodic function, the truncated sinusoid can be developed as a Fourier series. Since f(t) is an even function, the sine terms of the Fourier series vanish and we have

$$f(t)=\frac{a_0}{2}+\sum_{n=1}^{\infty} a_n\cos(n\omega_1 t) \tag{17}$$

with coefficients a_n given by

$$a_n = \frac{2}{T}\int_{-T/2}^{T/2} f(t)\cos(n\omega_1 t)dt \quad (18)$$

Specifically, for $n = 1$ this gives

$$a_1 = \frac{b}{\pi}\left(\theta - \frac{1}{2}\sin(2\theta)\right) \quad (19)$$

Accordingly, the Fourier transform of the truncated sinusoid is given by

$$\mathcal{F}(f)(\omega) = \frac{a_0}{2}\delta(\omega) + \sum_{n=1}^{\infty}\frac{a_n}{2}(\delta(\omega - n\omega_1) + \delta(\omega + n\omega_1)) \quad (20)$$

with δ the Dirac delta distribution. In particular

$$\mathcal{F}(f)(\omega_1) = \frac{a_1}{2}\delta(0) \quad (21)$$

When we now implicitely assume that we always work with a discrete Fourier transform of sampled time series, we can neglect the Dirac delta and write

$$A_T = |\mathcal{F}(f)(\omega_1)| = \frac{a_1}{2} \quad (22)$$

Eliminating b from (15) and (19) we derive the formula to calculate the mean $\overline{f(t)}$ from A_T as

$$\overline{f(t)} = 2A_T\frac{\sin(\theta) - \theta\cos(\theta)}{\theta - \frac{1}{2}\sin(2\theta)} \quad (23)$$

When f(t) should represent GPP, it must be zero during the night and this implies the following relation between θ and the relative fraction of light hours (f_{DL}) during a 24h period (Fig. 10).

$$\cos^{-1}(-a/b) = \theta = \pi f_{DL} \quad (24)$$

Resampling the estuarine model

For the resampling, we make use of a one year long velocity time series $v(t)$ generated by a one-dimensional hydrodynamic model of the Schelde estuary. We assume that this velocity is constant along the estuarine axis for the model domain over which the sensor is oscillating. The oscillating location of this sensor can then be calculated from this velocity time series as

$$x(t) = x_0 - \int_0^t v(\tau)d\tau \quad (25)$$

where x_0 is an arbitray location in the moving reference frame. As with the light forcing, this resampling is performed with each subset of 14 consecutive days of velocity data. The main advantage of this resampling approach is that we avoid the need for a computationally demanding tidally resolved reactive-transport model.

Contribution of lateral advection

A partial approximation of the contribution of lateral advection to diel fluctuations in the oxygen signal can be obtained from observed time series of salinity and observations of the spatial gradient of oxygen and salinity. We derive such approximation by starting from the transport equation of salinity (S) in a system with constant geometry

$$\frac{\partial S}{\partial t} = -v\frac{\partial S}{\partial x} + \frac{\partial}{\partial x}D\frac{\partial S}{\partial x} \quad (26)$$

where v is the water current and D is the dispersion coefficient. We can always write v as the sum of an average velocity and the velocity fluctuation due to the tide v_t. We assume that the average horizontal advection is in equilibrium with dispersion. Then the salinity gradient is constant, and the time evolution of salinity is the result of this gradient being moved back and forth with the tide, or

$$\frac{\partial S}{\partial t} = -v_t\frac{\partial S}{\partial x} \quad (27)$$

The Fourier-transform of this equation reads

$$i\omega\mathcal{F}(S) = -\mathcal{F}(v_t)\frac{\partial S}{\partial x} \quad (28)$$

This equation allows us to estimate the Fourier-amplitude of v_t based on a salinity time series and the observation of the salinity gradient. Combining this with observations of the oxygen gradient, we can estimate the Fourier-amplitude of the advective term of oxygen transport as

$$-\mathcal{F}(v_t)\frac{\partial O_2}{\partial x} = i\omega\mathcal{F}(S)\frac{\frac{\partial O_2}{\partial x}}{\frac{\partial S}{\partial x}} \quad (29)$$

This is an approximation of the error made by neglecting horizontal fluxes because it does not take into account diurnal fluctuations in the oxygen gradient. Also, the accuracy of spatial derivatives calculated from observations is limited, and determined by the spatial resolution of observations. Nevertheless, it will give an indication of the order of magnitude of the error associated with neglecting horizontal fluxes in a real-world estuarine situation.

References

Anonymous. 2011. The Astronomical Almanac for the year 2011. Data for astronomy, space sciences, geodesy, surveying, navigation and other applications. U.S. Governement Printing Office.

Batt, R. D., and S. R Carpenter. 2012. Free-water lake metabolism: Addressing noisy time series with a Kalman filter. Limnol. Oceanogr.: Methods **10**: 20–30. doi:10.4319/lom.2012.10.20

Bloomfield, P. 2000. Fourier analysis of time series, 2nd ed. Wiley.

Borges, A., B. Delille, L. Schiettecatte, F. Gazeau, G. Abril, and M. Frankignoulle. 2004a. Gas transfer velocities of CO2 in three European estuaries (Randers Fjord, Scheldt, and Thames). Limnol. Oceanogr. **49**: 1630–1641.

Borges, A., J. Vanderborght, L. Schiettecatte, F. Gazeau, S. Ferron-Smith, B. Delille, and M. Frankignoulle. 2004b. Variability of the gas transfer velocity of CO2 in a macrotidal estuary (the Scheldt). Estuaries **27**: 593–603. doi:10.1007/BF02907647

Champenois, W., and A. Borges. 2012. Seasonal and interannual variations of community metabolism rates of a posidonia oceanica seagrass meadow. Limnol. Oceanogr. **57**: 347–361. doi:10.4319/lo.2012.57.1.0347

Chen, C.-C., J. E. Petersen, and W. M. Kemp. 2000. Nutrient uptake in experimental estuarine ecosystems: Scaling and partitioning rates. Mar. Ecol. Prog. Ser. **200**: 103–116. doi:10.3354/meps200103

Ciavatta, S., R. Pastres, C. Badetti, G. Ferrari, and M. B Beck. 2008. Estimation of phytoplanktonic production and system respiration from data collected by a real-time monitoring network in the Lagoon of Venice. Ecol. Model. **212**: 28–36. doi:10.1016/j.ecolmodel.2007.10.025

Cole, J., M. Pace, S. Carpenter, and J. Kitchell. 2000. Persistence of net heterotrophy in lakes during nutrient addition and food web manipulations. Limnol. Oceanogr. **45**: 1718–1730. doi:10.4319/lo.2000.45.8.1718

Coloso, J. J., J. J. Cole, P. C. Hanson, and M. L. Pace. 2008. Depth-integrated, continuous estimates of metabolism in a clear-water lake. Can. J. Fish. Aquat. Sci. **65**: 712–722. doi:10.1139/f08-006

Coloso, J. J., J. J. Cole, and M. L. Pace. 2011. Difficulty in discerning drivers of lake ecosystem metabolism with high-frequency data. Ecosystems **14**: 935–948. doi:10.1007/s10021-011-9455-5

Desmit, X., J. P. Vanderborght, P. Regnier, and R. Wollast. 2005. Control of phytoplankton production by physical forcing in a strongly tidal, well-mixed estuary. Biogeosciences **2**: 205–218.

Eilers, P., and J. Peeters. 1988. A model for the relationship between light-intensity and the rate of photosynthesis in phytoplankton. Ecol. Model. **42**: 199–215. doi:10.1016/0304-3800(88)90057-9

Fahnenstiel, G., J. Chandler, H. Carrick, and D. Scavia. 1989. Photosynthetic characteristics of phytoplankton communities in lakes huron and michigan—p-i parameters and end-products. J. Great Lakes Res. **15**: 394–407. doi:10.1016/S0380-1330(89)71495-7

Folland, G. B. 1992. Fourier analysis and its applications. Brooks/Cole Publishing Company.

Gazeau, F., J. J. Middelburg, M. Loijens, J. P. Vanderborght, M. D Pizay, and J. P. Gattuso. 2007. Planktonic primary production in estuaries: Comparison of c-14, o-2 and o-18 methods. Aquat. Microb. Ecol. **46**: 95–106. doi:10.3354/ame046095

Gelda, R., and S. Effler. 2002. Metabolic rate estimates for a eutrophic lake from diel dissolved oxygen signals. Hydrobiologia **485**: 51–66. doi:10.1023/A:1021327610570

Grande, K., P. Williams, J. Marra, D. Purdie, K. Heinemann, R. Eppley, and M. Bender. 1989. Primary production in the North Pacific Gyre—a comparison of rates determined by the C-14,O-2 concentration and O-18 methods. Deep-Sea Res. Part A Oceanogr. Res. Pap. **36**: 1621–1634. doi:10.1016/0198-0149(89)90063-0

Guerrero, M., and R. Jones. 1996. Photoinhibition of marine nitrifying bacteria. I. Wavelength-dependent response. Mar. Ecol. Prog. Ser. **141**: 183–192. doi:10.3354/meps141183

Hanson, P. C., S. R. Carpenter, N. Kimura, C. Wu, S. P. Cornelius, and T. K. Kratz. 2008. Evaluation of metabolism models for free-water dissolved oxygen methods in lakes. Limnol. Oceanogr.: Methods **6**: 454–465. doi:10.4319/lom.2008.6.454

Harding, L. W. J., B. W Meeson, and T. R. J Fisher. 1986. Phytoplankton production in two east coast estuaries: Photosynthesis-light functions and patterns of carbon assimilation in chesapeake and delaware bays. Estuar. Coast. Shelf Sci. **23**: 773–806.

Holtgrieve, G. W., D. E. Schindler, T. A. Branch, and T. A'mar. 2010. Simultaneous quantification of aquatic ecosystem metabolism and reaeration using a bayesian statistical model of oxygen dynamics. Limnol. Oceanogr. **55**: 1047–1063. doi:10.4319/lo.2010.55.3.1047

Howarth, R., and A. F. Michaels. 2000. The measurement of primary production in aquatic ecosystems, p. 72–85. *In* O. Sala, R. Jackson, H. Mooney, and R. W. Howarth [eds.], Methods in ecosystem science. Springer-Verlag.

Howarth, R. W., R. Marino, R. Garritt, and D. Sherman. 1992. Ecosystem respiration and organic carbon processing in a large, tidally influenced river: The hudson river. Biogeochemistry **16**: 83–102. doi:10.1007/BF00002826

Jassby, A., and T. Platt. 1976. Mathematical formulation of the relationship between photosynthesis and light for phytoplankton. Limnol. Oceanogr. **21**: 540–547. doi:10.4319/lo.1976.21.4.0540

Kemp, W., and W. Boynton. 1980. Influence of biological and physical processes on dissolved-oxygen dynamics in an estuarine system—implications for measurement of community metabolism. Estuar. Coast. Mar. Sci. **11**: 407–431. doi:10.1016/S0302-3524(80)80065-X

Kester, D. R., M. F. Fox, and A. Magnuson. 1996. Modeling, measurements, and satellite remote sensing of biologically

active constituents in coastal waters. Mar. Chem. **53**: 131–145. doi:10.1016/0304-4203(96)00019-9

Kromkamp, J., and J. Peene. 1995. On the possibility of net primary production in the turbid schelde estuary (SW Netherlands). Mar Ecol. Prog. Ser. **121**: 249–259. doi:10.3354/meps121249

Kromkamp, J. C., and J. Peene. 2005. Changes in phytoplankton biomass and primary production between 1991 and 2001 in the westerschelde estuary (belgium/the netherlands). Hydrobiologia **540**: 117–126. doi:10.1007/s10750-004-7124-9

Langman, O. C., P. C. Hanson, S. R. Carpenter, and Y. H. Hu. 2010. Control of dissolved oxygen in northern temperate lakes over scales ranging from minutes to days. Aquat. Biol. **9**: 193–202. doi:10.3354/ab00249

Lauster, G., P. Hanson, and T. Kratz. 2006. Gross primary production and respiration differences among littoral and pelagic habitats in northern Wisconsin lakes. Can. J. Fish. Aquat. Sci. **63**: 1130–1141. doi:10.1139/f06-018

Marino, R., and R. W. Howarth. 1993. Atmospheric oxygen-exchange in the hudson riverdome measurements and comparison with other natural-waters. Estuaries **16**: 433–445. doi:10.2307/1352591

Markager, S., and K. Sand-Jensen. 1989. Patterns of night-time respiration in a dense phytoplankton community under a natural light regime. J. Ecol. **77**: 49–61. doi:10.2307/2260915

Obrador, B., P. A. Staehr, and J. Christensen. 2014. Vertical patterns of metabolism in three contrasting stratified lakes. Limnol. Oceanogr. **59**: 1228–1240. doi:10.4319/lo.2014.59.4.1228

Odum, H. 1956. Primary production in flowing waters. Limnol. Oceanogr. **1**: 102–117. doi:10.4319/lo.1956.1.2.0102

R Development Core Team. 2006. R: A language and environment for statistical computing. R foundation for statistical computing. ISBN 3-900051-07-0. doi:10.1007/s10985-007-9065-x

Riley, G. A. 1939. Plankton studies, II. The Western North Atlantic, May–June, 1939. J. Mar. Res. **2**: 145–162.

Sadro, S., J. M. Melack, and S. MacIntyre. 2011. Depth-integrated estimates of ecosystem metabolism in a high-elevation lake (emerald lake, sierra nevada, california). Limnol. Oceanogr. **56**: 1764–1780. doi:10.4319/lo.2011.56.5.1764

Sarthou, G., K. R. Timmermans, S. Blain, and P. TrÃ©guer. 2005. Growth physiology and fate of diatoms in the ocean: A review. J. Sea Res. **53**: 25–42. doi:10.1016/j.seares.2004.01.007

Shaw, P., and D. Purdie. 2001. Phytoplankton photosynthesis-irradiance parameters in the near-shore UK coastal waters of the North Sea: Temporal variation and environmental control. Mar. Ecol. Prog. Ser. **216**: 83–94. doi:10.3354/meps216083

Soetaert, K., P. Herman, and J. Middelburg. 1996. A model of early diagenetic processes from the shelf to abyssal depths. Geochim. Cosmochim. Acta **60**: 1019–1040. doi:10.1016/0016-7037(96)00013-0

Soetaert, K., and F. J. R. Meysman. 2011. ReacTran: Reactive transport modelling in 1D, 2D and 3D. R package version 1.3.2.

Soetaert, K., J. Middelburg, C. Heip, P. Meire, S. Van Damme, and T. Maris. 2006. Long-term change in dissolved inorganic nutrients in the heterotrophic Scheldt estuary (Belgium, The Netherlands). Limnol. Oceanogr. **51**: 409–423. doi:10.4319/lo.2006.51.1_part_2.0409

Soetaert, K., T. Petzoldt, and R. W. Setzer. 2010. Solving differential equations in R: Package desolve. J. Stat. Softw. **33**: 1–25.

Solomon, C. T., and others. 2013. Ecosystem respiration: Drivers of daily variability and background respiration in lakes around the globe. Limnol. Oceanogr. **58**: 849–866. doi:10.4319/lo.2013.58.3.0849

Staehr, P. A., and others. 2010. Lake metabolism and the diel oxygen technique: State of the science. Limnol. Oceanogr.: Methods **8**: 628–644. doi:10.4319/lom.2010.8.628

Staehr, P. A., J. M. Testa, W. M. Kemp, J. J. Cole, K. Sand-Jensen, and S. V. Smith. 2012. The metabolism of aquatic ecosystems: History, applications, and future challenges. Aquat. Sci. **74**: 15–29. doi:10.1007/s00027-011-0199-2

Steemann Nielsen, E. 1951. Measurement of the production of organic matter in the sea by means of carbon-14. Nature **167**: 684–685. doi:10.1038/167684b0

Swaney, D. P., R. W. Howarth, and T. J. Butler. 1999. A novel approach for estimating ecosystem production and respiration in estuaries: Application to the oligohaline and mesohaline Hudson River. Limnol. Oceanogr. **44**: 1509–1521. doi:10.4319/lo.1999.44.6.1509

Tobias, C. R., J. K. Boehlke, J. W. Harvey, and E. Busenberg. 2009. A simple technique for continuous measurement of time-variable gas transfer in surface waters. Limnol. Oceanogr.: Methods **7**: 185–195. doi:10.4319/lom.2009.7.185

Tsai, J.-W., and others. 2008. Seasonal dynamics, typhoons and the regulation of lake metabolism in a subtropical humic lake. Freshw. Biol. **53**: 1929–1941. doi:10.1111/j.1365-2427.2008.02017.x

Vallino, J., C. Hopkinson, and R. Garritt. 2005. Estimating estuarine gross production, community respiration and net ecosystem production: A nonlinear inverse technique. Ecol. Model. **187**: 281–296. doi:10.1016/j.ecolmodel.2004.10.018

Van Damme, S., and others. 2005. Spatial and temporal patterns of water quality along the estuarine salinity gradient of the Scheldt estuary (Belgium and The Netherlands): Results of an integrated monitoring approach. Hydrobiologia, **540**, 29–45. doi:10.1007/s10750-004-7102-2

Van de Bogert, M. C., D. L. Bade, S. R. Carpenter, J. J. Cole, M. L. Pace, P. C. Hanson, and O. C. Langman. 2012.

Spatial heterogeneity strongly affects estimates of ecosystem metabolism in two north temperate lakes. Limnol. Oceanogr. **57**: 1689–1700. doi:10.4319/lo.2012.57.6.1689

Westberry, T. K., P. J. L. B. Williams, and M. J. Behrenfeld. 2012. Global net community production and the putative net heterotrophy of the oligotrophic oceans. Global Biogeochem. Cycles **26**. doi:10.1029/2011GB004094

Williams, P., R. Raine, and J. Bryan. 1979. Agreement between the C-14 and oxygen methods of measuring phytoplankton production—reassessment of the photosynthetic quotient. Oceanol. Acta **2**: 411–416. doi:10.1029/2011GB004094

Submitted 26 October 2014
Revised 22 May 2015
Accepted 22 May 2015

Associate editor: Paul Kemp